Design, Analysis, and Construction of an Equal Split Wilkinson Power Divider

Logan J. Berens
Marquette University

DESIGN, ANALYSIS, AND CONSTRUCTION OF AN EQUAL SPLIT WILKINSON POWER DIVIDER

by

Logan J. Berens, B.S.

A Thesis submitted to the Faculty of the Graduate School,
Marquette University,
in Partial Fulfillment of the Requirements
for the Degree of Master of Science

Milwaukee, Wisconsin

August 2012

ABSTRACT
DESIGN, ANALYSIS, AND CONSTRUCTION OF AN EQUAL SPLIT WILKINSON POWER DIVIDER

Logan J. Berens, B.S.

Marquette University, 2012

The Wilkinson power divider is a well known device in the RF/microwave community used for splitting or combining signals. It is composed of simple transmission lines and a resistor, and takes advantage of the properties of quarter-wavelength transmission line sections to provide ideal power divider characteristics. Three different equal split Wilkinson power dividers are designed to operate near 1800 MHz and constructed using typical microstrip fabrication techniques. The three power dividers each feature a unique design to help determine how the microstrip layout can impact isolation and return loss. A circuit analysis of the general Wilkinson power divider schematic is performed to provide insight into the device characteristics as well as present a clear derivation of the correlating scattering matrix. A thorough comparison between the performances of each of the three different designs is conducted and the results are provided and discussed. The conclusions drawn from this investigation are that multiple Wilkinson power divider microstrip layouts can meet specific design criteria with similar results, indicating the robustness of the Wilkinson design. In particular and contrary to what is typically claimed within the RF/microwave community, a power divider featuring straight, parallel quarter-wavelength sections showed no degradation in isolation (or negligible effects of coupling) when compared to a power divider with curved quarter-wavelength sections.

ACKNOWLEDGEMENTS

Logan J. Berens, B.S.

I would like to begin by thanking my family for their continued support of my education and future career, and always urging me to do what I want to do. I certainly would not have made it this far without them. To the Marquette faculty, particularly the many professors I have gotten to know in the EECE department, I offer my deepest appreciation for your support and continued interest in my education. I am also incredibly grateful for the opportunity to have presented my thesis work at Marquette's Microwave Seminar, whose participants, especially Dr. Ishii, Dr. Wolski, Dr. Luglio, and Brian Petted, provided valuable insight and knowledge. Without their input this thesis would not be what it is today. Lastly, but certainly not least, I would like to thank my advisor, mentor, professor, and friend, Dr. James Richie. His wisdom and guidance has likely been the most critical to my thesis work, and his mentorship over the last three years has been a true privilege to experience.

TABLE OF CONTENTS

ACKNOWLEDGEMENTS i

LIST OF TABLES iv

LIST OF FIGURES v

Chapter I – Introduction 1

I.1 Motivation 1

I.2 Power Divider Background 2

I.2.1 The Scattering Matrix and Power Divider Characteristics 2

I.2.2 Power Divider Types and Properties 5

I.2.3 The Wilkinson Power Divider 8

I.3 Statement of the Problem 12

I.4 Outline 14

Chapter II – Theory & Design 15

II.1 Even-Odd Mode Analysis 15

II.1.1 Odd Mode 16

II.1.2 Even Mode 19

II.1.3 Incident and Reflected Voltages and the Scattering Matrix 22

II.2 Microstrip Dimensions and Calculations 23

II.2.1 Microstrip Background 23

II.2.2 Wilkinson Microstrip Dimensions 26

II.3 Wilkinson Power Divider Simulation and Desired Performance 27

Chapter III – Hand-Made Design, Discussion, and Results 31

III.1 Design 31

III.1.1 Introduction 31

III.1.2 AutoCAD Layout 32

III.2 Construction and Results 33

Chapter IV – Milled Designs: Discussion, Results, and Comparison 39

IV.1 Design 39

IV.1.1 Introduction 39

IV.1.2 AutoCAD Layouts and Dimensions 40

IV.2 Construction and Results 41

Chapter V – Discussion and Conclusions 52

V.1 Discusssion 52

V.2 Coupling and Isolation 53

V.3 Conclusions and Future Work 58

BIBLIOGRAPHY 61

LIST OF TABLES

Table 1: Isolation values for several values of n 12

Table 2: Odd Mode Voltages 19

Table 3: Even Mode Voltages 21

Table 4: Total Voltages 21

Table 5: Incident and Reflected Voltages 22

Table 6: Calculated Conductor Widths (mm) 27

Table 7: Expected Wilkinson Performance 30

Table 8: First Wilkinson Return Losses 35

Table 9: First Power Divider Total Bandwidth 38

Table 10: Milled Power Dividers Return Loss Comparison 45

Table 11: Milled Power Dividers Isolation Comparison 49

Table 12: Curved Power Divider Composite Frequency Range 49

Table 13: Step Power Divider Composite Frequency Range 49

Table 14: Straight Power Divider Composite Frequency Range 49

Table 15: Gap Spacing and Even-Odd Mode Impedances 54

LIST OF FIGURES

Figure 1: Lossless T-junction power divider 6

Figure 2: Resistive Power Divider 7

Figure 3: Transmission line circuit model for Wilkinson power divider 9

Figure 4: Wilkinson schematic with source at port two 15

Figure 5: Wilkinson with equivalent sources at ports two and three 16

Figure 6: Odd mode equivalent Wilkinson schematic with virtual ground 17

Figure 7: Top half circuit of Odd mode Wilkinson 17

Figure 8: Bottom half circuit of Odd mode Wilkinson 17

Figure 9: Simplified top half circuit of Odd mode Wilkinson 18

Figure 10: Even mode equivalent Wilkinson schematic with virtual open 19

Figure 11: Equivalent half circuit of Even mode Wilkinson 20

Figure 12: Simplified equivalent half circuit of Even mode Wilkinson 20

Figure 13: Microstrip Line 23

Figure 14: Cross-section of microstrip showing electric field 24

Figure 15: RFSim99 Wilkinson Schematic 28

Figure 16: Simulated Wilkinson S-Parameters vs. Frequency 29

Figure 17: First Wilkinson AutoCAD Layout 32

Figure 18: First Constructed Wilkinson Power Divider 33

Figure 19: First Wilkinson Port Return Losses 34

Figure 20: First Wilkinson Power Division 35

Figure 21: First Wilkinson Amplitude Balance 36

Figure 22: First Wilkinson Isolation 37

Figure 23: AutoCAD Layouts 40
Figure 24: Constructed Curved Wilkinson Power Divider 41
Figure 25: Constructed Step Wilkinson Power Divider 42
Figure 26: Constructed Straight Wilkinson Power Divider 42
Figure 27: Milled Power Dividers S11 Comparison 43
Figure 28: Milled Power Dividers S22 Comparison 43
Figure 29: Milled Power Dividers S33 Comparison 44
Figure 30: Milled Power Dividers Amplitude Balance 46
Figure 31: Milled Power Dividers Power Division 47
Figure 32: Milled Power Dividers Isolation 48
Figure 33: Gap Spacing vs. Coupling: Sonnet Simulation 54
Figure 34: Gap Spacing vs. Isolation: Sonnet Simulation 55
Figure 35: 5 mm Gap – Current Density Sonnet Simulation 56
Figure 36: 5 mm Gap – Current Density Zoomed In 56
Figure 37: 0.1 mm Gap – Current Density Sonnet Simulation 57
Figure 38: 0.1 mm Gap – Current Density Zoomed In 57
Figure 39: 0.1 mm Gap – Even Mode Operation 58

Chapter I – Introduction

I.1 Motivation

Within the RF and microwave community, power dividers have served a prominent role for years. The main function of a power divider is to split a given input signal into two or more signals as needed by the circuit/system. A typical application for a power divider is to split a signal to feed multiple low power amplifiers, and then have the signals from the amplifiers recombine into a high power output signal. Another power divider application and the inspiration for this thesis work, is within a phased antenna array system. In this system a signal is either fed through an equal split power divider featuring a specific number of output ports, or a series of equal split power dividers. The split signals are then fed through phase shifters and then to an array of transmitting antennas. The phase difference between each signal being transmitted allows for electronic beam scanning, allowing the transmitted beam to be focused in different directions depending upon the phase difference.

The goal of this thesis is to design, build, analyze, and better understand a power divider capable of operating in a phased antenna array system at 1800 MHz. However, the power divider constructed is an equal split two port device, while antenna arrays typically utilize more than two antennas. Consequently, if this power divider design were ever used in an antenna array, multiple power dividers would likely need to be used to split the signal into more than just two signals (i.e. 4, 8, 16, etc.) and further narrow or focus the beam.

I.2 Power Divider Background

I.2.1 The Scattering Matrix and Power Divider Characteristics

Before discussing different power dividers, it is important to first have an understanding of the scattering matrix and how it can be used to determine power divider characteristics. The scattering matrix, or S-matrix, is used to relate voltage waves incident on device ports to voltage waves reflected from device ports, taking into account both magnitude and phase. The S-matrix in terms of reflected voltage waves V^- and incident voltage waves V^+ can be written as [1-3]:

$$\begin{bmatrix} V_1^- \\ V_2^- \\ \vdots \\ V_N^- \end{bmatrix} = \begin{bmatrix} S_{11} & S_{12} & \cdots & S_{1N} \\ S_{21} & & & \vdots \\ \vdots & & & \\ S_{N1} & \cdots & & S_{NN} \end{bmatrix} \begin{bmatrix} V_1^+ \\ V_2^+ \\ \vdots \\ V_N^+ \end{bmatrix} \tag{1.1}$$

and simplified to:

$$[V^-] = [S][V^+] \tag{1.2}$$

Using these equations, each element of the S-matrix can be derived in terms of the appropriate incident and reflected voltage. The general equation for an element of the S-matrix can be defined as:

$$S_{ij} = \left.\frac{V_i^-}{V_j^+}\right|_{V_k^+ = 0 \; for \; k \neq j} \tag{1.3}$$

Essentially, an incident wave drives port *j* and a reflected wave exits port *i*, where the ratio of the reflected wave to incident wave provides the S-matrix element S_{ij}. Additionally, the incident waves on all ports other than port *j* are set equal to zero. A vector network analyzer is typically used to measure these parameters [1-3]. For devices

with more than two ports, such as a power divider (typically three ports), any ports not part of the measurement are terminated with a matched load.

When the device is matched at all ports, this implies that the input impedance seen at each port is equal to the characteristic impedance of the system. These equivalent impedances result in a reflection coefficient equal to zero, meaning that any wave incident on the matched port will not be reflected, or exit the port. Thus the reflected voltage at that port will be equal to zero. By applying (1.3) to the matched port (the S-matrix element where $i=j$), and knowing that the reflected voltage wave is equal to zero, it is clear that the S-matrix element must also be equal to zero. Furthermore, this implies that when a device is matched at each of its ports, the diagonal elements of its S-matrix reduce to zero [1-3].

One common characteristic found in power dividers as well as other devices is that of reciprocity. A reciprocal device is one in which the power transmitted between two ports of a network or device is the same regardless of the direction of propagation through the network or device. For a reciprocal device,

$$S_{ij} = S_{ji} \tag{1.4}$$

for all i and j. Based on this relationship between the S-matrix elements of a reciprocal device, a reciprocal device has a symmetrical S-matrix, or the S-matrix is equal to its transpose [1-3].

Another property of the S-matrix is how much loss can be attributed to the device itself. Ideally, a lossless power divider would be used in a system, however only low-loss dividers are physically realizable. It has been shown on multiple occasions, particularly

by Pozar [1], that if the S-matrix of a device is unitary, the device is lossless. Thus for a lossless device,

$$[S]^t[S]^* = [I] \tag{1.5}$$

where *I* is the identity matrix, the superscript *t* represents the transpose of the matrix and the superscript asterisk represents the conjugate of the matrix. Furthermore, a unitary matrix implies that the sum of the squares of the elements in a column of the matrix is equal to one [1-3].

Isolation between the output ports of a power divider is also critical to device performance. Isolation is characterized as the ability of a signal at one port to not affect, or be isolated from, the signal at another port. For a three port power divider, isolation between output ports two and three is important for reducing cross-talk that can be caused by coupling between the ports. In the S-matrix, the elements S_{23} and S_{32} are associated with the isolation between the output ports. These correspond to signals entering port two and exiting port three and vice versa. When the magnitudes of these elements are small, high isolation is achieved between the ports [1-3].

The ideal power divider would be lossless, or very low-loss, reciprocal, and easily matched at each port, however this is not possible. To demonstrate that any three-port power divider cannot be lossless, reciprocal, and matched, consider the generic S-matrix,

$$[S] = \begin{bmatrix} S_{11} & S_{12} & S_{13} \\ S_{21} & S_{22} & S_{23} \\ S_{31} & S_{32} & S_{33} \end{bmatrix} \tag{1.6}$$

First, the device is assumed to be matched at all ports and reciprocal. Based upon the definitions for the matched and reciprocal cases and how they apply to the S-matrix, the generic three-port S-matrix reduces to:

$$[S] = \begin{bmatrix} 0 & S_{12} & S_{13} \\ S_{12} & 0 & S_{23} \\ S_{13} & S_{23} & 0 \end{bmatrix} \quad (1.7)$$

For the lossless condition to be true, the matrix in (1.7) must be unitary and satisfy:

$$|S_{12}|^2 + |S_{13}|^2 = 1 \quad (1.8)$$

$$|S_{12}|^2 + |S_{23}|^2 = 1 \quad (1.9)$$

$$|S_{13}|^2 + |S_{23}|^2 = 1 \quad (1.10)$$

$$S_{13}^* S_{23} = 0 \quad (1.11)$$

$$S_{23}^* S_{12} = 0 \quad (1.12)$$

$$S_{12}^* S_{13} = 0 \quad (1.13)$$

This means that of the elements S_{12}, S_{13}, and S_{23}, two of them must be equal to zero in order to satisfy (1.11) – (1.13). For the sake of this analysis S_{12} and S_{13} are set equal to zero. However, it is clear that by setting these S-parameters equal to zero, (1.8) is not satisfied ($0 \neq 1$). Consequently, when two of the three elements S_{12}, S_{13}, and S_{23} are equal to zero, one of the equations (1.8) – (1.10) will not be satisfied, thus making a matched, reciprocal, lossless three port network impossible [1-3].

I.2.2 Power Divider Types and Properties

Although, an ideal (matched, reciprocal, and lossless) power divider is not physically realizable, there are power dividers that demonstrate two of the three properties. T-junction dividers, resistive dividers, and the Wilkinson power divider are three common power dividers featuring unique characteristics. These power dividers can

be constructed using various types of transmission lines (i.e. waveguides, microstrip, or stripline) or using resistive networks.

The lossless T-junction power divider, for example, is simply three transmission lines connected at a single junction. This junction has a reactance associated with it due to fringing fields and higher order modes. Figure 1 shows a transmission line model of the lossless T-junction [1].

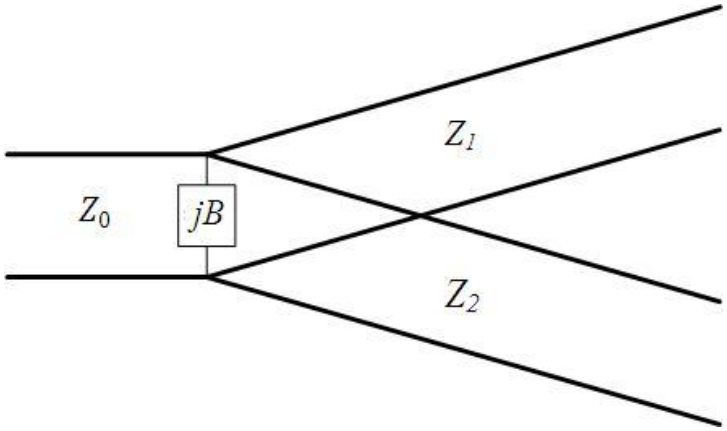

Figure 1: Lossless T-junction power divider

The impedances of the three lines of the T-junction are related by

$$\frac{1}{Z_0} = \frac{1}{Z_1} + \frac{1}{Z_2} + jB \tag{1.14}$$

where Z_0 is the characteristic impedance of the input line, Z_1 and Z_2 are the characteristic impedances of both output lines, and B is the reactance created at the junction of the three lines. Thus, given an input impedance, the two output impedances can be matched to the input impedance. Typically the reactance B is not negligible, but can be reduced with the use of another reactive tuning element. This allows (1.14) to be reduced to:

$$\frac{1}{Z_0} = \frac{1}{Z_1} + \frac{1}{Z_2} \tag{1.15}$$

Since the transmission lines are very low loss, (1.15) can be used to determine the necessary impedances of each transmission line to yield various ratios of power division [1].

The lossless T-junction is capable of being reciprocal, but has the drawbacks of lacking isolation between the output ports and an inability to be matched at all ports. Eqn. (1.15) demonstrates the inability to be matched at all ports, because the impedances of at least two of the three transmission lines will need to differ in order to achieve the chosen power division. Consequently, matching techniques such as the quarter-wave transformer need to be implemented to maintain a matched system [1].

Resistive power dividers can be implemented to ensure that the same impedance is achieved at all ports, however loss is then introduced to the power divider. Figure 2 shows a typical resistive power divider model [1].

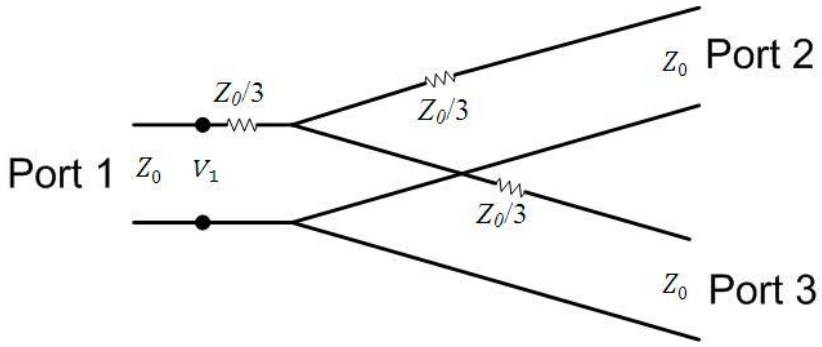

Figure 2: Resistive Power Divider

For a resistive divider, the input power is given by

$$P_{IN} = \frac{1}{2}\frac{V_1^2}{Z_0} \tag{1.16}$$

and in the equal split case the output powers at ports two and three are

$$P_2 = P_3 = \frac{1}{2}\frac{(1/2\,V_1)^2}{Z_0} = \frac{1}{8}\frac{V_1^2}{Z_0} \tag{1.17}$$

Summing P_2 and P_3 gives the total output power at the two ports. This gives a value equal to half of the input power, demonstrating that half of the input power was dissipated by the resistors. Furthermore, isolation between the output ports is not necessarily achieved with the resistive power divider [1].

I.2.3 The Wilkinson Power Divider

The Wilkinson power divider, proposed by Ernest Wilkinson in 1960 provides isolation between the output ports, is capable of being matched at all ports, and becomes lossless when the output ports are matched [4]. Figure 3 shows the equivalent transmission line circuit for a Wilkinson power divider, where the power delivered to the two output ports is equal [1]. The design of the Wilkinson divider is composed of a transmission line (typically microstrip or stripline) that has been split into a specific number of transmission lines, each one quarter-wavelength long. In Wilkinson's original proposal, a shorting plate is used at the input to connect each of the transmission lines. Resistors are connected between each output transmission line and a common junction. When the outputs are connected to matched loads for an equal split Wilkinson, the voltages along each output transmission line are of the same magnitude and phase. This causes the connecting resistors to have no voltage drop across them, and consequently, dissipate no power [4].

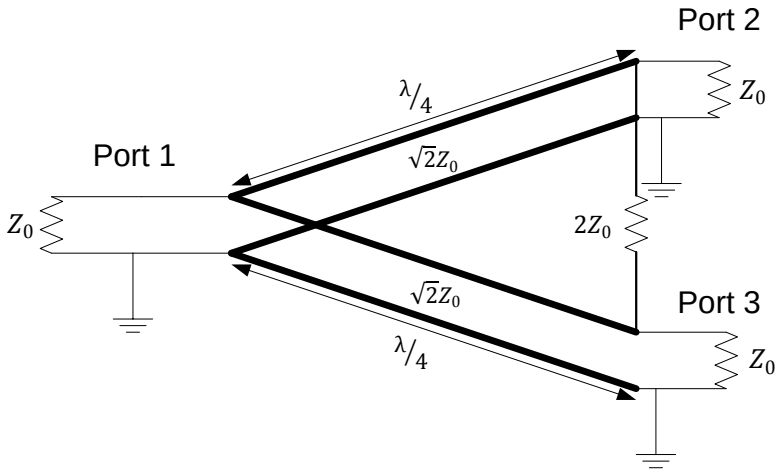

Figure 3: Transmission line circuit model for Wilkinson power divider

The necessary impedance of each quarter-wave transmission line is equal to the characteristic impedance of the input transmission line multiplied by a factor of $\sqrt{2}$, as shown in Figure 3. Additionally, the internal resistor that connects the two output ports is equal to the characteristic impedance of the input transmission line multiplied by a factor of two. These impedances allow the outputs of the Wilkinson power divider to be isolated and matched, while also allowing the input to the power divider to be matched [4]. The ideal scattering matrix of the Wilkinson power divider with matched loads is:

$$S = \frac{-j}{\sqrt{2}}\begin{bmatrix} 0 & 1 & 1 \\ 1 & 0 & 0 \\ 1 & 0 & 0 \end{bmatrix} \tag{1.18}$$

The *S* matrix shows that as power enters port one, it gets equally divided into ports two and three. The matched ports of the divider sets S_{11}, S_{22}, and S_{33} equal to zero. Since the power divider is lossless when a signal is applied to port one, the magnitude (sum of the square of each element) of column one of the *S* matrix is equal to one (the unitary, condition) [1].

It should be noted that when a signal is applied at port two, only half of the power of the incident signal is observed at port one. This implies that half of the initial power is dissipated through the resistor, but reciprocity is achieved ($S_{21} = S_{12}$). Furthermore, due to the isolation between ports two and three, no power is observed at port three when power is applied at port two for an ideal Wilkinson (S_{23} and S_{32} are set equal to zero).

The Wilkinson power divider is also capable of handling reflections in the system quite effectively. A reflection at an output port is essentially the equivalent of applying a signal at an output port. The reflected signal travels back to the other output port through two paths: one path through the resistor, and a second path through the initial input junction. Since the transmission lines are quarter-wave lengths, the signal through the resistor arrives at a specific phase, while the signal traveling along the two quarter-wave lines (two 90° phase shifts) arrives 180° out of phase. When these out of phase reflections are of equal amplitude, they result in complete cancellation (the isolation between the output ports) [5].

If two signals of equal amplitude and phase are applied simultaneously to the two output ports of an equal split Wilkinson, the sum of the signals will be observed at port one (typically the input port). Since the signals are of equal amplitude and phase, the resistor will see the same potential at each port, and no power will be dissipated. Once the signals arrive at the junction they will constructively interfere, and the power divider acts as a power combiner.

For unequal power division using the Wilkinson power divider, there is a particular set of design equations that can be used to determine the impedances of the

quarter-wave sections and the connecting resistor. These impedances are dictated by the value of *K*, given by

$$K = \sqrt{\frac{P_3}{P_2}} \tag{1.19}$$

where P_2 and P_3 are the desired powers at ports two and three respectively. The impedance for the quarter-wave transmission line connected to port three is then given by

$$Z_{03} = Z_0 \sqrt{\frac{1 + K^2}{K^3}} \tag{1.20}$$

Similarly, the impedance for the transmission line connected to port two is given by

$$Z_{02} = K^2 Z_{03} = Z_0 \sqrt{K(1 + K^2)} \tag{1.21}$$

and the value of the connecting resistor is

$$R = Z_0(K + 1/K) \tag{1.22}$$

When the ratio of the output powers are equal to one (equal power division), the impedances reduce to those seen previously in Figure 3 [1].

Wilkinson power dividers can either be cascaded to achieve multiple output ports, thus maintaining the isolation between ports, or a single Wilkinson power divider can incorporate more than two equal power output ports. Under these circumstances, (1.19) – (1.22) are not useful because they are based upon the power ratio between only two output ports. For a given number of output ports *n*, an output load impedance R_L, and an input impedance R_S the characteristic impedance of each quarter-wave section, $Z_{\lambda/4}$, is given by [5]:

$$Z_{\lambda/4} = \sqrt{nR_L R_S} \tag{1.23}$$

Addtionally,

$$R = R_L \tag{1.24}$$

demonstrating that the resistors that connect between the output ports and the common junction are simply equal to the load impedances at each output.

These equations can be used to develop a Wilkinson power divider with *n* output ports, each delivering a power equal to 1/*n* multiplied by the input power. It should be noted that as the number of output ports increases, the isolation between the ports goes down. Table 1 gives ideal isolation values between *n* number of output ports [5].

N	**Isolation (dB)**
2	∞
3	∞
4	21.6
5	19.5
6	17.6
7	17.2
8	16.1
10	14.9
12	14.1

Table 1: Isolation values for several values of n

Due to the lossless nature of the Wilkinson power divider under matched conditions, and the relative ease in which it can be matched, it is obvious that the Wilkinson provides the most well-rounded power divider performance. Additionally, it can be easily constructed using microstrip, making it an ideal choice to investigate further in this thesis.

I.3 Statement of the Problem

Countless Wilkinson power dividers have been designed and constructed, particularly in recent years due to more sophisticated simulation software and simplified

fabrication techniques (i.e. microstrip). Furthermore, novel Wilkinson designs have been developed that allow unequal division with large division ratios [6], as well as dual and broadband frequency operation [7] [8]. Designs that take advantage of coupling between the quarter-wave transmission lines to reduce layout size while maintaining a good bandwidth have also been developed [9]. This thesis does not necessarily seek to develop a novel device, but to design, build, analyze, and better understand a microstrip Wilkinson power divider capable of equally splitting the power of a signal at 1800 MHz.

Using RFSim99, a simple RF circuit simulator, an idealized Wilkinson can be simulated to help determine realistic values for return loss, isolation, etc. However, RFSim99 does not inherently take into account the effects that junction or taper reactance can have on such parameters, as well as the center frequency and bandwidth. In this thesis, multiple Wilkinson designs are built and measured with a vector network analyzer to get a better understanding of how different microstrip layouts impact device performance.

A divider featuring straight, parallel quarter-wave sections is designed, built, and compared to a divider featuring curved quarter-wave sections. A claim within the RF community is that a power divider featuring straight, parallel quarter-wave sections will be more susceptible to the negative effects of coupling (degradation in isolation) than a power divider featuring curved quarter-wave sections [9]. By building these two devices, a reasonable comparison can be performed and the effects of coupling in both devices can be determined. Similarly, a divider featuring a step junction instead of a continuous taper between impedances is also constructed and analyzed. This device was built to determine

if a step junction would result in a degradation of return loss when compared to a device with a taper.

I.4 Outline

Chapter II of this thesis covers the even-odd mode circuit analysis of the Wilkinson power divider to help better understand its performance characteristics and derive its scattering matrix. A brief discussion on the theory and mathematics of microstrip is presented and how it applies to the design and dimensions of the power divider microstrip layouts. Simple simulations and ideal Wilkinson power divider performance are also presented to get a better idea of the limitations of the device. Chapter III discusses the design, construction, and results of the hand-made Wilkinson power divider. Chapter IV discusses the knowledge gained from the previous design and how it was used to improve the next designs. It also presents the design, construction, and results of three unique, machine fabricated Wilkinson power dividers and how their performance compares to the previous design as well as between one another. The final chapter helps to validate the results obtained and provides a brief discussion on the conclusions drawn from this study and potential future work.

Chapter II – Theory & Design

II.1 Even-Odd Mode Analysis

The Wilkinson power divider's design and functionality can be analyzed by performing an even-odd mode analysis. This analysis utilizes superposition and circuit symmetry to solve for incident and reflected voltages. Once these voltages are obtained, the scattering matrix of the Wilkinson can be derived [10].

Initially, a Wilkinson featuring a source of value V_S at port two is considered, while ports one and three are terminated with loads of impedance Z_0**.** Figure 4 shows the circuit schematic of the Wilkinson. For simplicity, the bottom conductor of each transmission line is removed in upcoming schematics [10].

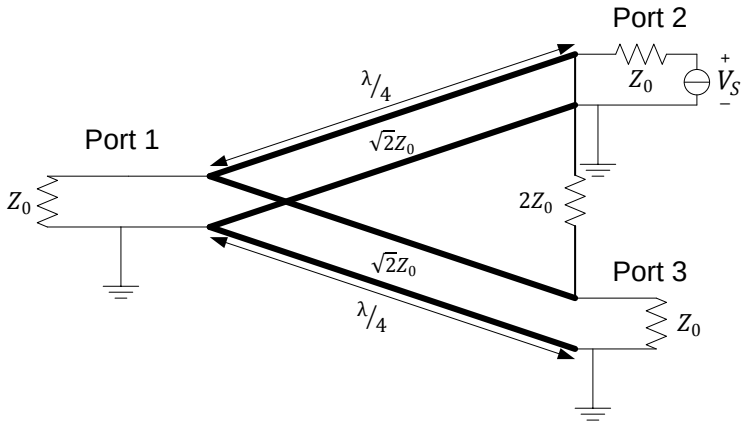

Figure 4: Wilkinson schematic with source at port two

The circuit can be redrawn with the source at port two, V_S, split into two sources in series, each with a value of $V_S/2$. Additionally, two voltage sources can be drawn at port three, $V_S/2$ and $-V_S/2$. Figure 5 shows the schematic with the new voltage sources. The voltages V_1, V_2, and V_3 represent the total incident and reflected voltages at each port (necessary for deriving the scattering matrix) [10].

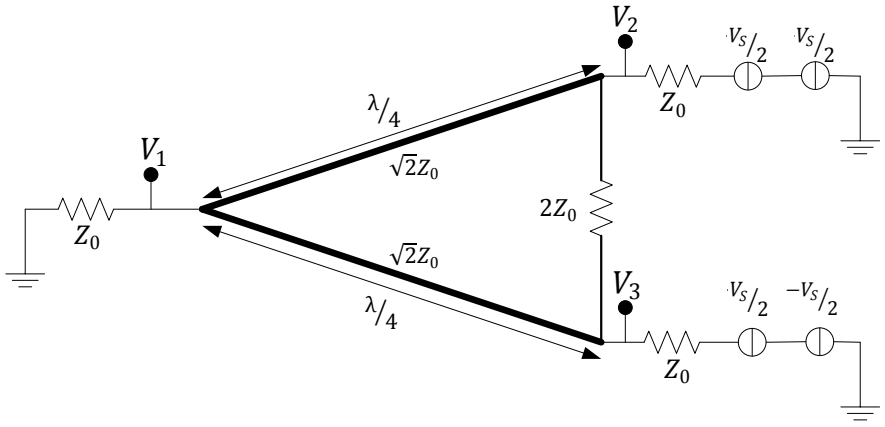

Figure 5: Wilkinson with equivalent sources at ports two and three

II.1.1 Odd Mode

When a positive source ($V_S/2$) is turned off at each output port, the circuit has odd symmetry. Since the voltage sources at ports two and three are 180° out of phase, they cancel along the circuit's plane of symmetry (the plane that bisects the circuit into two equivalent sub-circuits). This cancellation results in a virtual ground along the plane of symmetry. Figure 6 shows the resulting equivalent circuit with the plane of symmetry. For the sake of analysis, the resistor at port one can be split into two resistors in parallel, each with a value $2Z_0$. V_1 can be split into separate nodes schematically, but these points are technically still the same node (no voltage difference between the two points). Consequently, a short circuited line can be drawn between the two V_1 nodes. The resistor between ports two and three can be split into two series resistors each with a value of Z_0. Additionally, the voltages V_1, V_2, and V_3 now represent the total voltage from the odd mode analysis and are denoted with a superscript "O" [8].

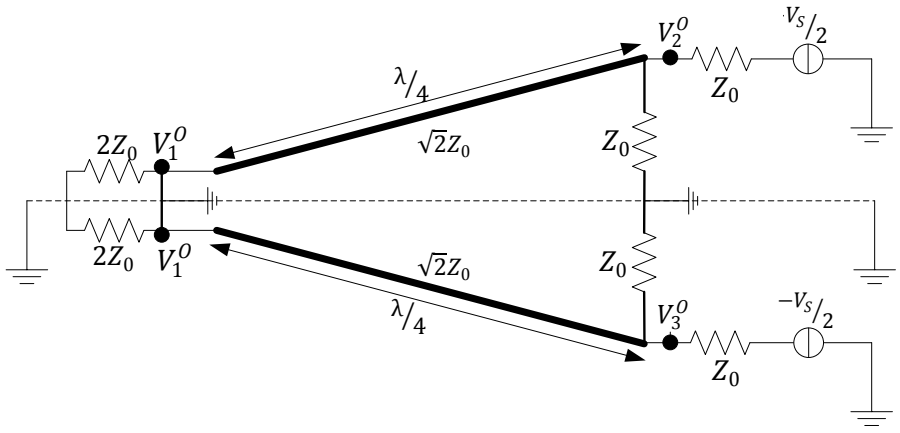

Figure 6: Odd mode equivalent Wilkinson schematic with virtual ground

The top and bottom halves of Figure 6 can then be redrawn as two individual circuits utilizing the plane of symmetry from the previous figure as an equivalent ground. The only difference between the two circuits is the phase of the voltage source. These circuits are shown in Figure 7 and Figure 8 with the bottom conductors of the transmission lines redrawn to provide a better visual representation of the schematic [10].

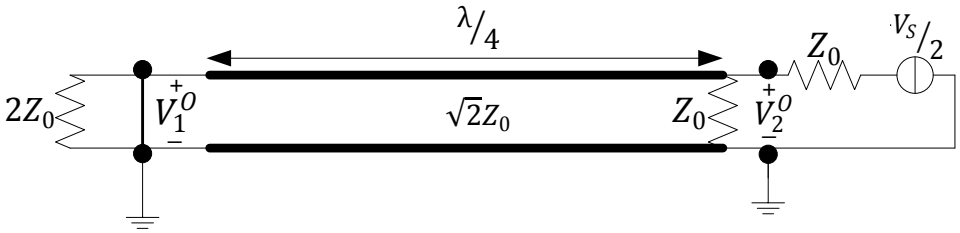

Figure 7: Top half circuit of Odd mode Wilkinson

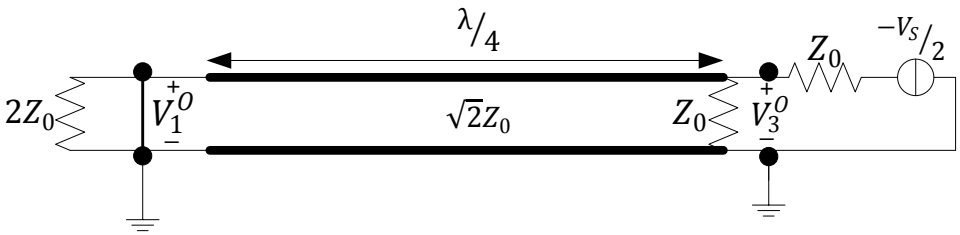

Figure 8: Bottom half circuit of Odd mode Wilkinson

Since the transmission line is terminated with a short circuit, the impedance $2Z_0$ can be disregarded because no current will flow through that component. The voltage V_1^O is equal to zero due to the short circuited line [10]. The input impedance of the short circuit and the quarter-wave transmission line can be found with:

$$Z_{IN} = Z_C \frac{Z_L + jZ_C \tan \beta l}{Z_C + jZ_L \tan \beta l} \tag{2.1}$$

where Z_L is the load impedance (in this case zero due to the short circuited line) and Z_C is the characteristic impedance of the transmission line (in this case $\sqrt{2}Z_0$), and β is $2\pi/\lambda$ [11]. Furthermore, the quarter-wave transmission line ($l=\lambda/4$) allows (2.1) to reduce to:

$$Z_{IN} = \frac{Z_C^2}{Z_L} \tag{2.2}$$

The short circuit load (Z_L) causes the equivalent impedance to go to infinity, or an open circuit. The sub-circuit shown in Figure 7 is redrawn in Figure 9 with the short circuit and transmission line converted to the open circuit [11].

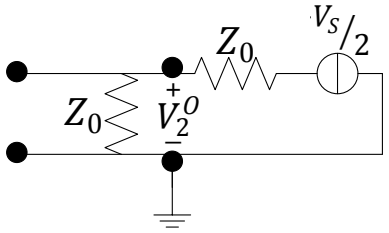

Figure 9: Simplified top half circuit of Odd mode Wilkinson

The odd mode voltage for V_2 can be easily obtained by doing some simple voltage division. In this case V_2^O is equal to $V_S/4$. Likewise, V_3^O is equal to $-V_S/4$ due to the out of phase voltage source for the other sub-circuit. Each of the total voltages associated with the odd mode have now been found. These values are shown in Table 2 [10].

Port Voltage	Voltage Value
V_1^O	0
V_2^O	$V_S/4$
V_3^O	$-V_S/4$

Table 2: Odd Mode Voltages

II.1.2 Even Mode

Next the even mode voltages need to be found. Beginning with the circuit shown in Figure 5, a positive voltage source is turned off at port two and the negative voltage source is turned off at port three. Under this condition, the two sources that are left at the output ports are equivalent. Due to the equivalent voltages, there is no current flow along the plane of symmetry (again the plane that bisects the circuit). The lack of current flow implies that a virtual open exists along the plane of symmetry. Figure 10 shows the equivalent even mode circuit with the virtual open. Similar to the odd mode analysis, the resistor at port one has been split into two resistors in parallel, and the resistor between ports two and three has been split into two resistors in series. Notice that the voltage points are now denoted with a superscript "E" to represent the total voltage associated with the even mode at each respective point [10].

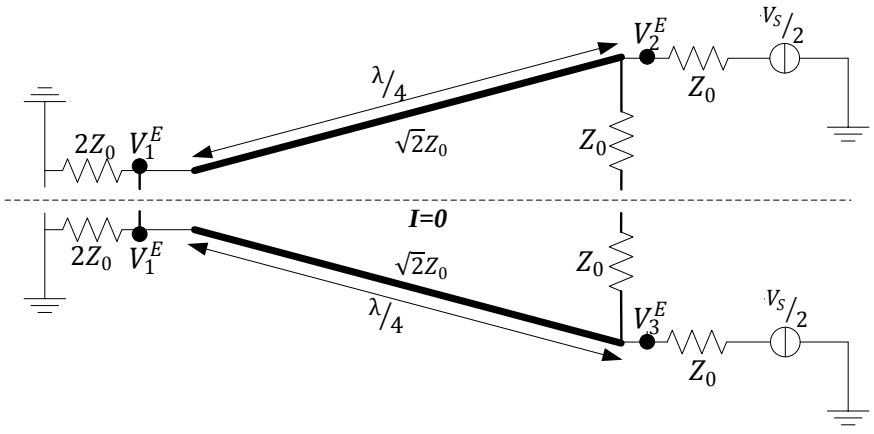

Figure 10: Even mode equivalent Wilkinson schematic with virtual open

Similar to the odd mode analysis, there are two individual circuits that can be drawn from Figure 10. Since the voltage sources are equivalent, along with the rest of the components and values, the circuits are identical. Also, Figure 10 shows that the resistors between ports two and three are essentially disconnected (terminated by the open circuit plane of symmetry) and can therefore be removed from the sub-circuits. Figure 11 shows the equivalent sub-circuit for the even mode analysis [10].

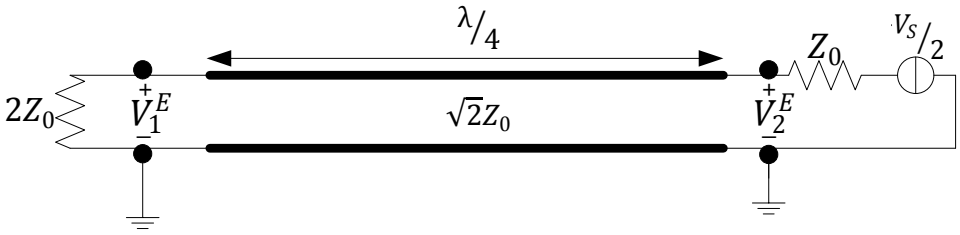

Figure 11: Equivalent half circuit of Even mode Wilkinson

By using (2.1) the $2Z_0$ load impedance and quarter-wave transmission line can be reduced to an equivalent input impedance of Z_0. Figure 12 shows the simplified sub-circuit.

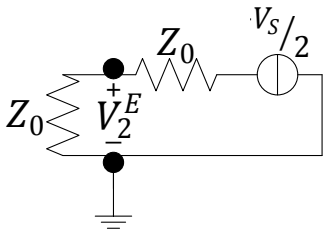

Figure 12: Simplified equivalent half circuit of Even mode Wilkinson

This simplified circuit is identical to the one shown in Figure 9 in the odd mode analysis. Consequently, the voltage for V_2^E is equal to $V_S/4$. Since both sub-circuits for the even mode analysis are identical, V_3^E is also equal to $V_S/4$ [10].

Now V_1^E needs to be determined, however it is not quite as easily obtained as the other voltages. By examining the circuit shown in Figure 11, it can be seen that V_1^E is equal to the voltage drop across the load $2Z_0$. By using

$$V(z') = I_L(Z_L \cos \beta z' + Z_C j \sin \beta z') \quad (2.3)$$

the voltage at any point *z'* can be solved for in terms of the current flowing through the load, I_L, the load impedance, Z_L, and the characteristic impedance of the transmission line, Z_C. Additionally, *z'* is the distance away from the load (i.e. to find the voltage at the load, *z'* is set equal to zero), and β is $2\pi/\lambda$ [9]. The current, I_L, can be solved for by realizing that V_2^E is equal to the voltage when *z'* is equal to $\lambda/4$, which is $V_S/4$. By substituting this value in for *V(z')*, setting Z_L equal to $2Z_0$, and Z_C equal to $\sqrt{2}Z_0$, I_L can be calculated to be $-V_s j/(4\sqrt{2}Z_0)$. Using this calculated value of I_L and by setting *z'* equal to zero (while using the same values for load and characteristic impedance), *V(z'=0)* = V_1^E is $-V_s j/(2\sqrt{2})$. The total voltage values at each port for the even mode analysis have now been determined as shown in Table 3 [10].

Port Voltage	Voltage Value
$\boldsymbol{V_1^E}$	$-V_s j/(2\sqrt{2})$
$\boldsymbol{V_2^E}$	$V_S/4$
$\boldsymbol{V_3^E}$	$V_S/4$

Table 3: Even Mode Voltages

Since the even-odd mode analysis takes advantage of superposition, the voltages at each node for each analysis can be summed to get the total voltage at each respective node. Table 4 shows the results of the total voltages [10].

Port Voltage	Voltage Values	Total Voltage
$\boldsymbol{V_1}$	$-V_s j/(2\sqrt{2}) + 0$	$-V_s j/(2\sqrt{2})$
$\boldsymbol{V_2}$	$V_S/4 + V_S/4$	$V_S/2$
$\boldsymbol{V_3}$	$V_S/4 + -V_S/4$	0

Table 4: Total Voltages

II.1.3 Incident and Reflected Voltages and the Scattering Matrix

The total voltage for each port has been derived for a source placed at port two. The incident and reflected voltages now need to be determined. Ports one and three are matched in the original schematic in Figure 4 making the incident voltages at these ports equal to zero. Similarly, the source at port two is matched making the reflected voltage at port two also equal to zero. Table 5 shows the incident and reflected voltages at each port, given a matched source at port two and matched loads at ports one and three [10].

Port	Incident Voltage (V^+)	Reflected Voltage (V^-)
1	0	$-V_s j/(2\sqrt{2})$
2	$V_S/2$	0
3	0	0

Table 5: Incident and Reflected Voltages

Using this information, the second column of the scattering matrix can be derived. The values for the second column of the S-matrix are determined.

$$S_{12} = \frac{V_1^-}{V_2^+} = \frac{-jV_S}{2\sqrt{2}} * \frac{2}{V_s} = \frac{-j}{\sqrt{2}} \tag{2.4}$$

$$S_{22} = \frac{V_2^-}{V_2^+} = 0 * \frac{2}{V_s} = 0 \tag{2.5}$$

$$S_{32} = \frac{V_3^-}{V_2^+} = 0 * \frac{2}{V_s} = 0 \tag{2.6}$$

The rest of the S parameters can be determined through circuit inspection. Due to the bilateral symmetry of the Wilkinson, applying a source at port three instead of port two will yield equivalent S-parameters for the third column of the matrix. Therefore S_{12} will equal S_{13}, S_{22} will equal S_{33}, and S_{32} will equal S_{23}. If a matched source is applied to port one with matched terminations at ports two and three, the values for S_{21} and S_{31} can be shown to be equivalent to S_{12} and S_{13} due to the reciprocal nature of the Wilkinson.

Furthermore, the matched source at port one implies that S_{11} will be equal to zero. Thus, the S-matrix of the Wilkinson power divider has been derived and confirmed [10].

$$S = \frac{-j}{\sqrt{2}}\begin{bmatrix} 0 & 1 & 1 \\ 1 & 0 & 0 \\ 1 & 0 & 0 \end{bmatrix} \tag{2.7}$$

II.2 Microstrip Dimensions and Calculations

II.2.1 Microstrip Background

Microstrip transmission lines are commonly used to build power dividers among other devices, because it can be easily fabricated through various techniques such as photolithography or milling. Additionally, it can be used for a wide frequency range, spanning from below 1 GHz up to tens of GHz. The microstrip layout shown in Figure 13 is composed of a dielectric substrate between a ground plane and thin conductor where W is the conductor width, D is the thickness of the dielectric substrate, and ε_r is the relative permittivity of the substrate [1].

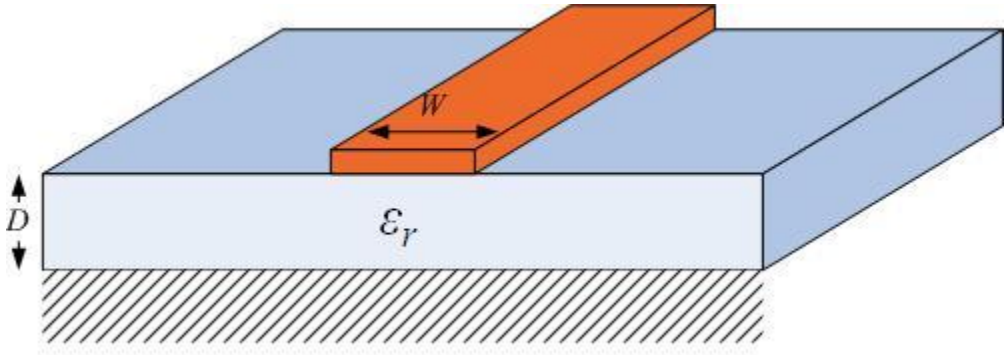

Figure 13: Microstrip Line

In the absence of a dielectric, only air would separate the conductor and ground plane, resulting in a simple TEM (transverse-electromagnetic) transmission line. Due to

the dielectric and the region of air above the substrate and the conductor, microstrip lines do not support a true TEM mode of propagation. In most cases however, the substrate thickness is much smaller than a wavelength, and the fields propagating along the microstrip are quasi-TEM, or very similar to TEM propagation [1]. Figure 14 shows typical field lines for the main transverse electric field in a microstrip line [12].

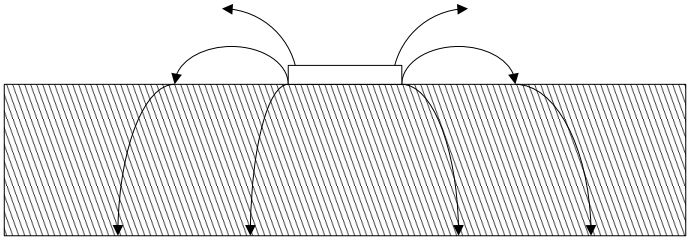

Figure 14: Cross-section of microstrip showing electric field

In order to design a Wilkinson power divider using microstrip, certain characteristics of the microstrip line must be determined such as phase velocity, propagation constant, wavelength, and conductor width. Approximations for the phase velocity v_p and propagation constant β for the microstrip line are given as

$$v_p = \frac{c}{\sqrt{\varepsilon_{eff}}} \tag{2.8}$$

$$\beta = k_0\sqrt{\varepsilon_{eff}} \tag{2.9}$$

where c is the speed of light, k_0 is the propagation constant for free space ($\omega\sqrt{\mu_0\varepsilon_0}$), and ε_{eff} is the effective dielectric constant for the substrate and the air [1]. The effective dielectric constant is a function of the relative permittivity of the substrate, the substrate thickness, and the conductor width. It can be approximately determined using:

$$\varepsilon_{eff} = \frac{\varepsilon_r + 1}{2} + \frac{\varepsilon_r - 1}{2} * \left(\frac{1}{\sqrt{1 + 12D/W}}\right) \tag{2.10}$$

The wavelength, λ_m (in millimeters) in the microstrip is related to the phase velocity and can be determined using:

$$\lambda_m = \frac{300}{F\sqrt{\varepsilon_{eff}}} \tag{2.11}$$

where F is the intended frequency of operation in GHz [12].

The characteristic impedance of a microstrip line is also related to the conductor width and dielectric thickness. More conveniently, the ratio of conductor width to dielectric thickness can be determined for a given characteristic impedance and relative permittivity using the following equations given by Pozar [1]:

$$\frac{W}{D} = \begin{cases} \dfrac{8e^A}{e^{2A}-2} & for\ \dfrac{W}{D} < 2 \\ \dfrac{2}{\pi}\left[B - 1 - ln(2B-1) + \dfrac{\varepsilon_r - 1}{2\varepsilon_r}\left\{\ln(B-1) + 0.39 - \dfrac{0.61}{\varepsilon_r}\right\}\right] & for\ \dfrac{W}{D} > 2 \end{cases} \tag{2.12}$$

where

$$A = \frac{Z_0}{60}\sqrt{\frac{\varepsilon_r + 1}{2}} + \frac{\varepsilon_r - 1}{\varepsilon_r + 1}\left(0.23 + \frac{0.11}{\varepsilon_r}\right) \tag{2.13}$$

and

$$B = \frac{377\pi}{2Z_0\sqrt{\varepsilon_r}} \tag{2.14}$$

These equations are based on the work done by Hammerstad [13]. Similar design equations are also provided by Edwards [12].

II.2.2 Wilkinson Microstrip Dimensions

The first Wilkinson design in this study was built using a single-sided copper clad RT Duroid 5870 board from Rogers Corporation and hand cut copper tape traces to act as the microstrip conductor, while later iterations were constructed from milling double-sided copper clad RT Duroid 5870. The relative permittivity and loss tangent, per Rogers Corporation, of the RT Duroid 5870 is 2.33 and 0.0005, respectively. For the first build, the substrate thickness is 62 mils or 1.575 mm and the thickness of the copper tape is 31.75 μm. The skin depth of the copper was calculated to be approximately 1.5 μm at 1800 MHz (1/20 the copper tape thickness and 1/10 the copper thickness on the milled boards.) It is important to have a skin depth much smaller than the conductor thickness to maintain a low effective resistance of the conductor.

Using these parameters and knowing that the desired characteristic impedance for the input and output traces is 50 Ω, the necessary conductor width could be calculated using Rogers Corporation's MWI 2010 microstrip calculator [14, 15]. The calculator uses the ideas presented by Hammerstad [13] and others [16, 17, 18] to provide accurate calculations. Furthermore, using (2.12) and (2.13) the necessary conductor width was calculated by hand to verify the results from the MWI 2010 calculator. The same process was done for determining the conductor width of the quarter-wave sections of the Wilkinson.

The MWI 2010 calculator was then used to determine the microstrip thicknesses when using the double-sided RT Duroid 5870 board. The only parameter that differed was the conductor thickness (17 μm for the copper on the double-sided board instead of

31.75 μm for the copper tape). Table 6 shows the various calculated conductor widths in mm.

Calculation	Width for 50Ω (mm)	Width for 70.7Ω (mm)
Single-Side by Hand	4.68	2.67
Single-Side by MWI	4.665	2.634
Double-Side by MWI	4.689	2.658

Table 6: Calculated Conductor Widths (mm)

The values shown in Table 6 show a good correlation between the hand calculated widths and MWI 2010 widths. Since the first Wilkinson design was constructed using hand-cut copper traces, the widths chosen for that design were 4.64 mm and 2.64 mm to help account for inaccuracies in the cutting process. These widths were also chosen for the milled double-sided designs for the sake of consistency.

The last parameter that needed to be determined was the length of the quarter-wave transmission line sections. The effective permittivity of the copper quarter-wave sections on the RT Duroid 5870 was calculated using (2.10). Based upon the previously calculated microstrip dimensions, 2.64 mm was used for the conductor width and 1.575 mm was used for the substrate thickness, and the effective permittivity was calculated to be approximately 1.9. Using (2.11), the quarter-wave length necessary for the Wilkinson to have a center frequency at 1800 MHz is equal to 30.23 mm.

II.3 Wilkinson Power Divider Simulation and Desired Performance

Despite having isolated output ports and functioning as a lossless divider when the ports are matched, the quarter-wave sections of the Wilkinson make it a narrowband, or frequency dependent device. The frequency responses of several S-parameters for a Wilkinson power divider were simulated in RFSim99, to determine the ideal

performance. To achieve a center frequency of 1.8 GHz, a phase velocity of 218 Mm/s was used (calculated from eqn. 2.8) and the quarter-wave sections were the necessary 30.23 mm in length. The characteristic impedance of the input and output transmission lines was chosen to be 50 Ω. The impedance of the quarter-wave sections was 70.7 Ω and the connecting resistor was 100 Ω. The RFSim99 schematic is shown in Figure 15.

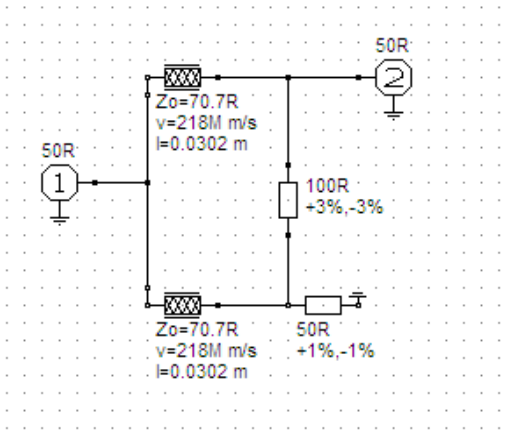

Figure 15: RFSim99 Wilkinson Schematic

The simulation results for the magnitudes of S_{11}, S_{21}, S_{22}, and S_{23} in dB are plotted in Figure 16. The center frequency for each parameter is approximately 1800 MHz, confirming the calculations for the phase velocity in the microstrip and the quarter-wave length sections. Additionally, near 1800 MHz the return losses for S_{11} and S_{22} both exceed 50 dB, or very near a reflection coefficient of zero. Similarly, S_{23} has a transmission coefficient that is close to zero, implying high isolation between ports two and three. The equal-split nature of the Wilkinson is confirmed because S_{21} is essentially 3 dB (50% power delivered from port one to port two) across the band.

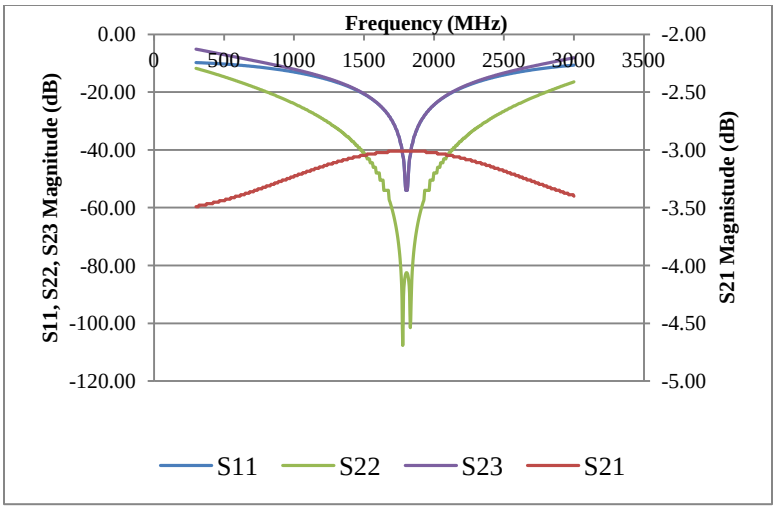

Figure 16: Simulated Wilkinson S-Parameters vs. Frequency

Typical device parameters that can be measured are bandwidth, input and output port return losses, isolation between output ports, and amplitude and phase balances and ripples. Manufactured Wilkinson power dividers have been shown to achieve bandwidths up to 65:1, although these feature multiple quarter-wave sections. The bandwidths for manufactured power dividers are typically defined as having a VSWR less than 1.5:1 [19]. This VSWR is equal to a return loss of approximately 13.5 dB. Across the bandwidth isolation values around 20 dB are typical, with values above 15 dB considered good. The amplitude balance (how evenly the power is split) is typically less than +/-0.25 dB, depending on the bandwidth of the device [19].

One equal-split Wilkinson power divider available for purchase features input and output VSWR less than 1.2:1, an amplitude balance less than +/-0.2 dB, and a minimum isolation of 22 dB over a frequency range of 0.7-2.7 GHz [20]. These values demonstrate how well a typical Wilkinson power divider can function when manufactured professionally.

Since at least one Wilkinson power divider was constructed by hand, the layout tolerances will be much higher than what would be found from a manufactured power divider. Consequently, the expected performance parameters will likely not meet the values typical for manufactured Wilkinson power divider's previously described. Ideally, the measured center frequency for the port return losses should fall within +/- 100 MHz of the desired frequency, in this case 1800 MHz.

Based upon the specifications for manufactured power dividers, the bandwidth will be defined as the spectrum of frequencies that fall below a 1.4:1 VSWR (>15 dB return loss). The simulation results in Figure 16 show that the bandwidth for a VSWR of 1.4:1 is approximately 1200-2400 MHz. Consequently, a reasonable bandwidth to expect from the power divider should be 1300-2300 MHz. Across this bandwidth the magnitude of S_{21} fluctuates between 3 and 3.1 dB, resulting in an ideal amplitude balance well within +/-0.25 dB of manufacturing tolerances. However, a more realistic amplitude balance to expect, particularly for a hand-cut divider, would be within +/-0.4 dB. Table 7 indicates the expected values that the Wilkinson should achieve for specific parameters over the bandwidth.

Parameter	Expected Value
Return Losses	>15 dB (97% Power Transmitted)
Isolation	>15 dB
Amplitude Balance	+/- 0.4 dB

Table 7: Expected Wilkinson Performance

Chapter III – Hand-Made Design, Discussion, and Results

III.1 Design

III.1.1 Introduction

As discussed in the previous chapter, the first Wilkinson power divider was constructed by hand with copper tape and single-sided copper clad RT Duroid 5870 board. However, the lengths of the quarter-wave transmission lines were mistakenly calculated to be too short (27.30 mm) by using the relative permittivity of the substrate ($\varepsilon_r = 2.33$) in (2.11) instead of the effective permittivity of the air and substrate ($\varepsilon_{eff} = 1.9$). The length of the quarter-wavelength sections should be 30.23 mm for an operating frequency near 1800 MHz when using the appropriate effective permittivity. Due to this error, the constructed device is expected to have an operating frequency higher than the intended design.

Although the frequency of operation for the device was unintentionally shifted up, this initial design provided information on how the physical start and end points of the quarter-wavelength sections correlate to the center frequency of the device. Without the use of sophisticated simulation software, it is difficult to gauge exactly where the quarter-wavelength sections begin and end. Not knowing these points with certainty can result in significant measurement differences (in this case up to 5 mm). Furthermore, the effect that the microstrip junction would have on frequency of operation and other device characteristics was also difficult to determine. The results from the first design helped to determine more accurate quarter-wavelength start and end points for the next designs as well as show that a reasonable Wilkinson power divider could be constructed by hand.

III.1.2 AutoCAD Layout

The first Wilkinson design was drawn in AutoCAD 2011 and is shown in Figure 17.

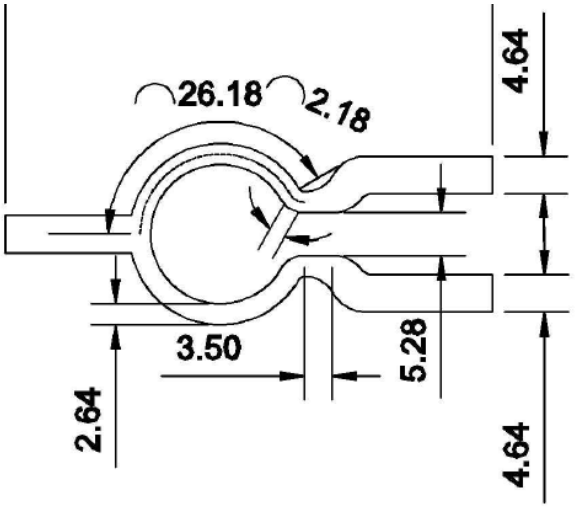

Figure 17: First Wilkinson AutoCAD Layout

A Wilkinson power divider featuring curved quarter-wavelength sections was initially drawn due to its relative popularity, though a later design utilizes straight sections to compare performance between the two. The widths, based on the microstrip calculations in Chapter II, of the 50Ω and 70.7Ω lines are 4.64 mm and 2.64 mm, respectively. A larger chip resistor (6.4 mm x 3.2 mm x 0.6 mm) was chosen to simplify the soldering process. The chip resistor size dictated how far away the two output lines could be separated, in this case 5.28 mm. A tapered transmission line was drawn between the quarter-wavelength sections and the 50Ω output lines to potentially mitigate reflections in the device (another design featuring step junctions between the two transmission lines is constructed and measured to verify this).

The quarter-wavelength sections can be considered to be between 23.84 mm and 28.36 mm, depending upon the start and end points (the intended length is 27.30 mm as previously discussed). Using (2.11) this correlates to a potential center frequency between 1920 and 2280 MHz.

III.2 Construction and Results

The design was constructed by laying a piece of copper tape over the single-sided RT Duroid 5870 board. The AutoCAD layout was placed over the copper tape, and the design was carefully cut around. The chip resistor was soldered in place by using solder paste and a heat gun. 50Ω SMA connectors were then soldered to the ends of the ports. The constructed Wilkinson is shown in Figure 18.

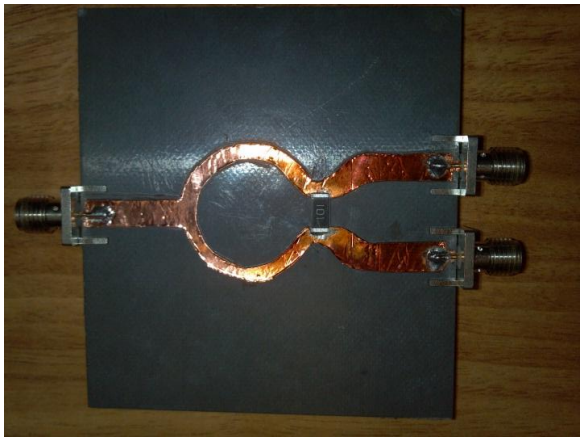

Figure 18: First Constructed Wilkinson Power Divider

Once the Wilkinson was constructed, the Agilent 8714ES vector network analyzer (VNA) was used to measure the various S-parameters. The VNA was calibrated, and the return loss associated with each port was measured while any unused ports were

terminated with 50Ω loads. The power divider was measured between 600 and 3000 MHz (the upper frequency limit for the VNA) to be sure to cover the entire band of operation for the device. The results for the return loss at each port are shown in Figure 19.

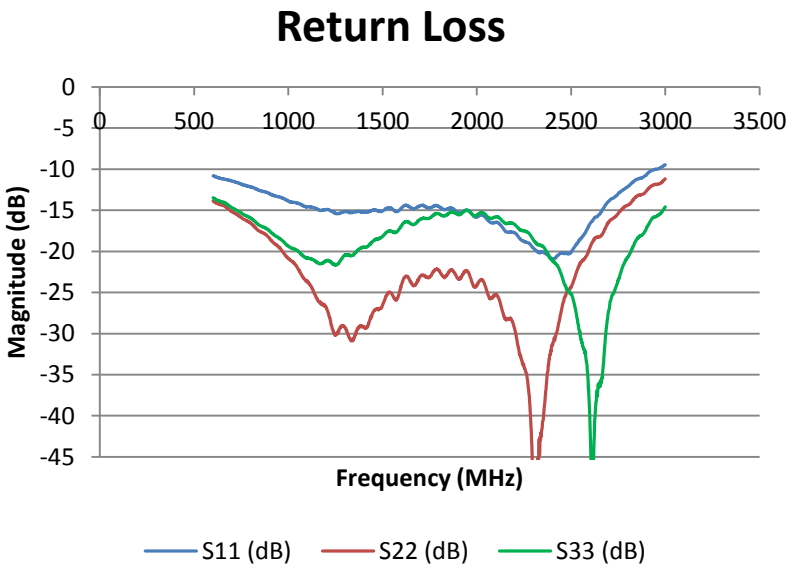

Figure 19: First Wilkinson Port Return Losses

The results in Figure 19 show a shift between the center frequencies of each return loss measurement. This is likely due to the inaccuracies of the cutting process leading to a device that is not quite symmetrical. As shown in Chapter II, the symmetry of the Wilkinson power divider is critical to ensuring proper operation. However the deep nulls for S_{22} and S_{33}, and the 20 dB return loss for S_{11} offer encouraging results showing that a very low loss matched power divider can be constructed by hand. Table 8 shows the maximum return loss achieved at each port, the frequency at which the maximum return loss occurred, and the band over which it performed within the previously defined 15 dB minimum (a maximum VSWR of 1.4 across the band).

S-Parameter	Center Frequency (MHz)	Max Return Loss (dB)	Band > 15 dB (MHz)
S11	2370	21.0	1920-2660
S22	2330	76.5	700-2780
S33	2645	56.0	1900-3000

Table 8: First Wilkinson Return Losses

The center frequency for each of these return losses is still slightly higher than what was previously predicted (between 1920 and 2280 MHz). The center frequencies for S_{11} and S_{22} are close to the high end of the predicted band. These results indicate that the shortest measurement made on the AutoCAD layout for the quarter-wavelength sections best corresponds to the electrical length of the sections.

The rest of the S-parameters were measured using the VNA in a similar fashion. Since the Wilkinson power divider is a reciprocal device, S_{12} should equal S_{21}, S_{13} should equal S_{31}, and S_{23} should equal S_{32}. Figure 20 shows the values for S_{12}, S_{21}, S_{13}, and S_{31} from 600-3000 MHz.

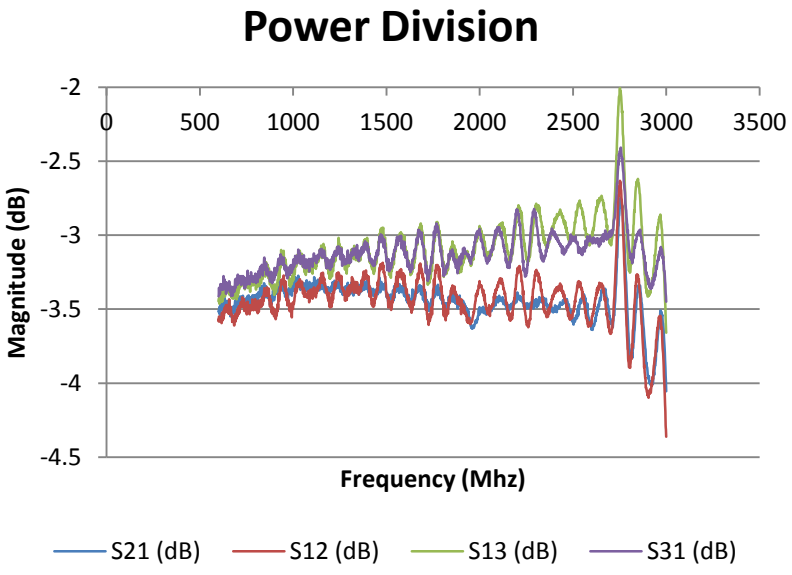

Figure 20: First Wilkinson Power Division

The results in Figure 20 show similar responses between S_{12} and S_{21} and likewise S_{13} and S_{31}, indicating that the device is reciprocal. Figure 20 also indicates that the power divider does not quite evenly divide the power. Since S_{21} approximately fluctuates between 3.3 and 3.7 dB, and S_{31} approximately fluctuates between 2.8 and 3.4 dB, more power is delivered to port three than port two (approximately 45% and 49% power delivered to ports two and three respectively). The bandwidth over which these fluctuations occur is approximately 600 – 2700 MHz. By taking the difference between S_{31} and S_{21}, the amplitude balance between the two outputs can be determined. Figure 21 shows the amplitude balance of the hand-made Wilkinson.

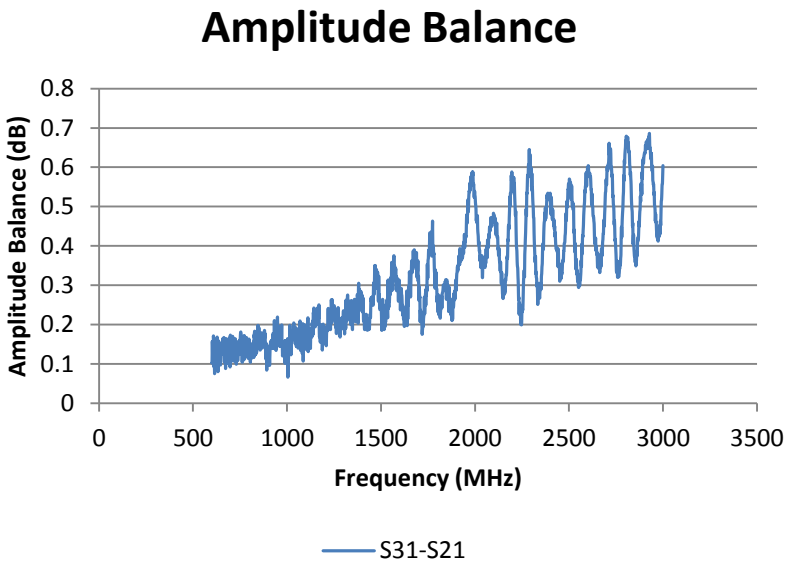

Figure 21: First Wilkinson Amplitude Balance

These results are a direct result of the inaccuracies in the hand cut traces of the Wilkinson. The quarter-wavelength section leading to port two was cut narrower than intended, leading to a slightly higher impedance than the section leading to port three. Consequently, the difference in impedance between the two quarter-wavelength sections

caused not only an unequal power split, but also contributed to a small amount of loss in the resistor (based on the analysis in Chapter II there would be no loss if the device was perfectly symmetric and matched). Although an amplitude balance below 0.4 was originally deemed acceptable in Chapter II, the obvious difference between the widths of the two quarter-wave length sections makes an amplitude balance below 0.6 more indicative of the bandwidth of the power-split. Based on Figure 21, an amplitude balance below 0.6 is reliably achieved from approximately 600-2290 MHz.

The isolation between ports two and three is shown in Figure 22.

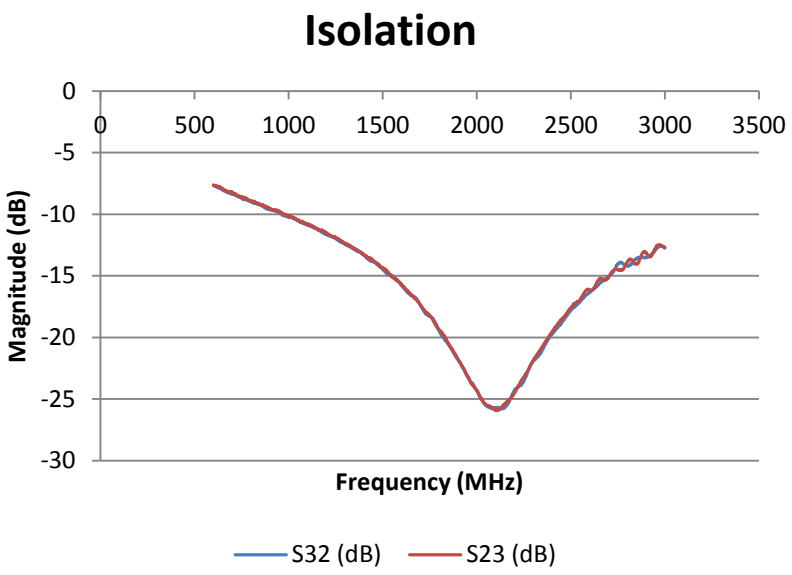

Figure 22: First Wilkinson Isolation

Figure 22 shows that the results for S_{23} and S_{32} are essentially identical, further demonstrating the reciprocal nature of the Wilkinson. The frequency at which the isolation reaches a maximum value (26 dB) is approximately 2100 MHz. Additionally, the divider provides good isolation (>20 dB) between 1820 and 2370 MHz.

The overall results of the first hand made Wilkinson although not ideal, acted as a good indicator of what realistic values to expect from later device builds. The

operational bandwidth of the device can be determined by looking at the bandwidth of the return losses, the amplitude balance, and the isolation. These results are compared in Table 9.

Parameter	Low Frequency (MHz)	High Frequency (MHz)
S11 Return Loss	1920	2660
S22 Return Loss	700	2780
S33 Return Loss	1900	3000
S31/S21 Amplitude Balance	600	2290
S23/S32 Isolation	1820	2370

Table 9: First Power Divider Total Bandwidth

Based on the results in Table 9, the total device bandwidth for the hand-made Wilkinson is approximately 1920 – 2290 MHz. Although this is a very small bandwidth, ($\approx$ 400 MHz instead of 1000 MHz as was hoped for in Chapter II) a reciprocal device featuring good isolation and good return loss values was constructed relatively easily by hand nonetheless. With careful cutting the device can maintain a good deal of symmetry, potentially mitigating the frequency shifts between return losses and improving the amplitude balance of the device. Additionally, the center frequency results, particularly from the return losses, provided more information on how to define the quarter-wavelength sections for the upcoming builds.

Chapter IV – Milled Designs: Discussion, Results, and Comparison

IV.1 Design

IV.1.1 Introduction

Using the knowledge gained from the hand-cut Wilkinson power divider, three more power dividers were built using an LPFK milling machine and CircuitCAM 4.0 software. The first power divider (to be identified as the "curved" power divider henceforth and shown in Figure 23.b) featured the same layout as the hand-cut power divider, but with longer quarter-wave length sections to bring down the frequency of operation of the device to 1800 MHz. The next power divider (to be identified as the "step" power divider and shown in Figure 23.a) featured the same quarter-wave length sections as the curved power divider, but utilized step junctions between the 50Ω and 70.7Ω sections instead of a continuous taper. The reason for building the step power divider was primarily to determine if there would be a significant impact on any of the return losses when compared to the curved power divider. The final power divider featured straight, parallel quarter-wave length sections (to be identified as the "straight" power divider and shown in Figure 23.c) and the same continuous taper as the curved power divider. This Wilkinson power divider was built to help determine the extent to which coupling between quarter-wave length sections would impact performance, primarily isolation. Once the performance of each of the power dividers was measured with the vector network analyzer, a discussion and investigation on the performance and effects of microstrip step junctions and coupled lines was done to help verify the results.

IV.1.2 AutoCAD Layouts and Dimensions

Similar to the first hand-cut Wilkinson power divider, the layouts for the next three power dividers were created using AutoCAD 2011. Each layout is shown in Figure 23.

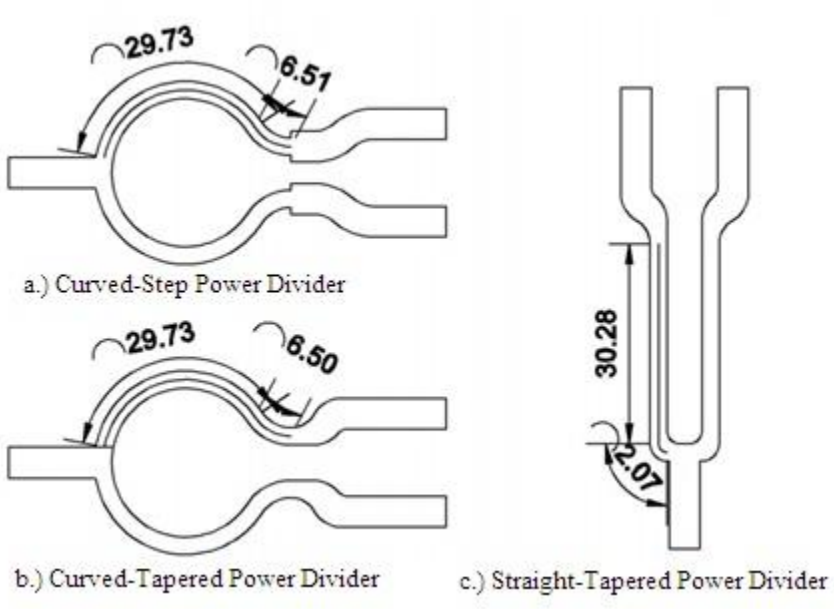

Figure 23: AutoCAD Layouts

Since the physical lengths of the quarter-wave length sections of the first hand-made power divider corresponded to center frequencies lower than what was actually measured, longer quarter-wave length sections (approximately 36 mm for the curved power dividers and 32 mm for the straight power divider instead of the necessary 30 mm) were used to further lower the frequency of operation. The length of the quarter-wave length sections is the only dimension that differs between the hand-made and curved power divider. The step power divider employs a step junction immediately after the quarter-wavelength section, maintaining the same quarter-wavelength dimension as the

curved power divider. The straight power divider's quarter-wavelength sections are separated by a distance determined by the spacing between the resistor pads (5.28 mm).

IV.2 Construction and Results

Each of the power dividers was built from RT Duroid 5870 board featuring double-sided rolled ½ ounce copper (17 μm thickness). The AutoCAD layouts were converted to gerber files and then milled using an LPFK PCB routing machine, removing the excess copper around the designs. The depth at which the machine milled the copper was set by hand introducing a small source of construction error. However, there was far greater symmetry in each of these devices than in the hand-made power divider. The resistors were then soldered to the copper traces using solder paste and a heat gun. The constructed Wilkinson power dividers are shown in Figure 24, Figure 25, and Figure 26.

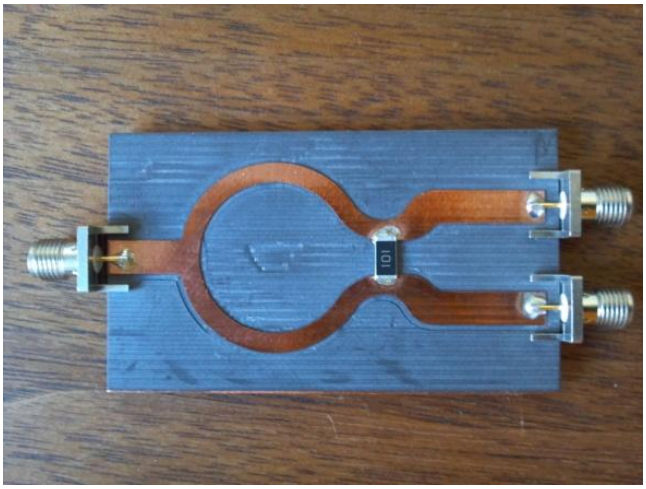

Figure 24: Constructed Curved Wilkinson Power Divider

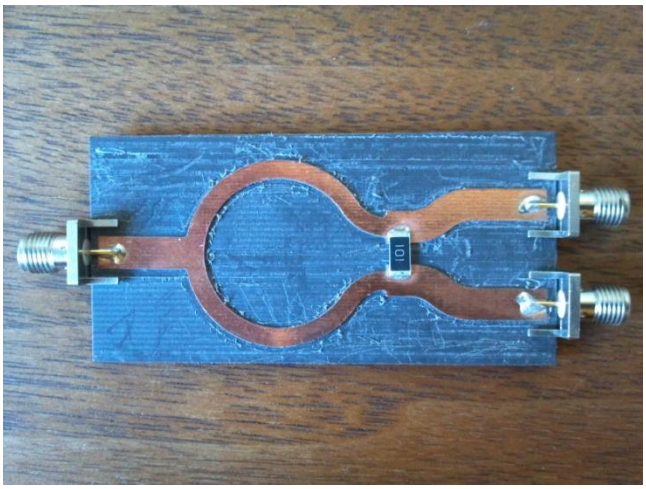

Figure 25: Constructed Step Wilkinson Power Divider

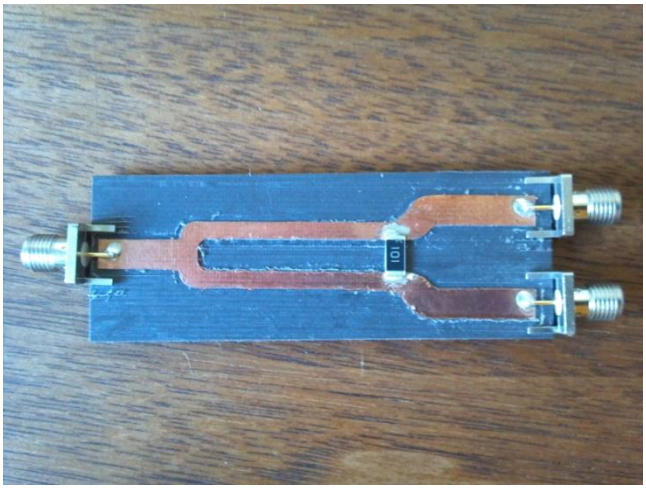

Figure 26: Constructed Straight Wilkinson Power Divider

Similar to the hand-made power divider, the S-parameters for each of the devices was obtained using the Agilent 8714ES vector network analyzer. The VNA was calibrated, and the return loss associated with each port was measured while any unused ports were terminated with 50Ω loads. The same frequency range (600-3000 MHz) was used for the sake of consistency.

The return losses for each of the milled power dividers are shown in Figure 27, Figure 28, and Figure 29.

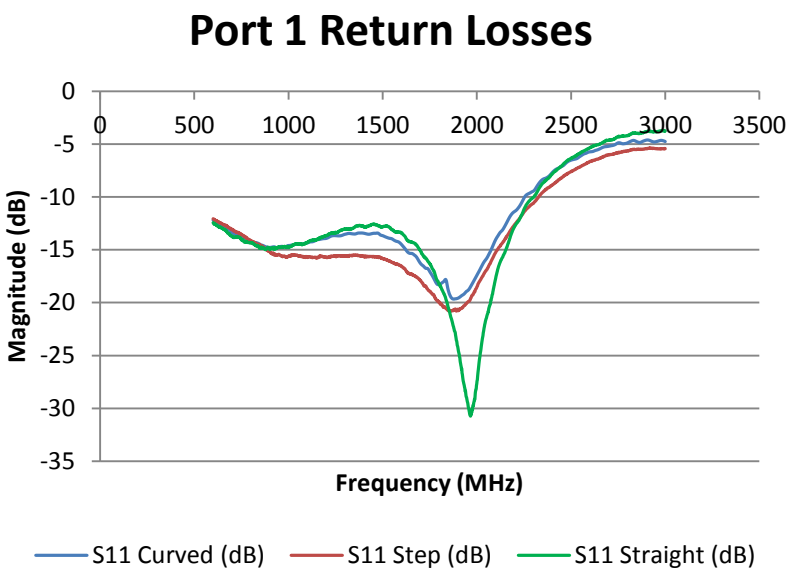

Figure 27: Milled Power Dividers S11 Comparison

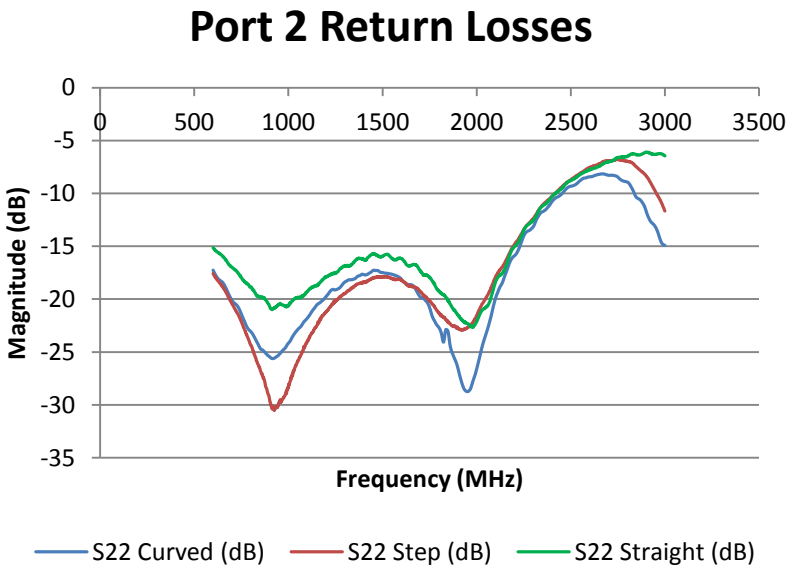

Figure 28: Milled Power Dividers S22 Comparison

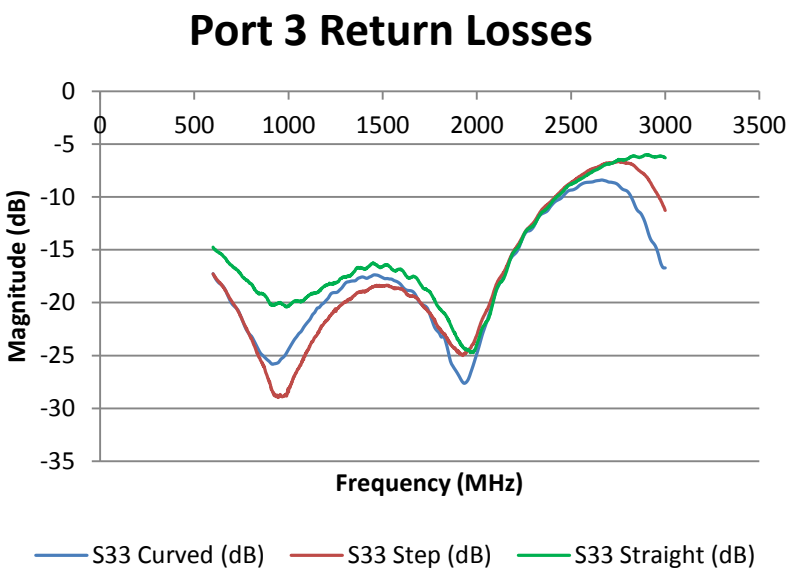

Figure 29: Milled Power Dividers S33 Comparison

Based on these figures it is easy to see that the increased quarter-wave length sections did bring down the port one center frequency (in this case defined as the high-frequency null) of the devices (approximately 1870 MHz for the curved and step power dividers and 1970 MHz for the straight power divider). The straight power divider still had a center frequency higher than the curved and step power dividers, which makes sense because it featured quarter-wavelength sections approximately 4 mm shorter than the other dividers. The straight power divider also featured a port one return loss of about 30 dB at the center frequency, while the others were at approximately 20 dB, perhaps due to the smaller T-junction. Additionally, the results for S_{22} and S_{33} are very similar for each of the power dividers, indicating that these devices are much more symmetrical than the hand-made device.

Table 10 shows the center frequency for each return loss on each power divider, the maximum return loss achieved, and the band over which the return loss was greater than 15 dB.

Power Divider	S-Parameter	Center Frequency (MHz)	Max Return Loss (dB)	Band > 15 dB (MHz)
Curved	S11	1870	19.5	1620-2080
Step	S11	1865	20.5	890-2110
Straight	S11	1970	30.5	1690-2160
Curved	S22	1930	28.5	600-2220
Step	S22	1920	23.0	600-2200
Straight	S22	1940	22.0	600-2200
Curved	S33	1930	27.5	600-2230
Step	S33	1920	25.0	600-2200
Straight	S33	1970	24.5	600-2200

Table 10: Milled Power Dividers Return Loss Comparison

These results show a very similar performance between all three power dividers, particularly between the curved and step power dividers. Although the step power divider incorporated a step junction, it is clear that there was little to no difference between the return loss characteristics for the curved power divider and the step power divider. This leads to the conclusion that the use of a step junction in this particular device is just as effective as a continuous taper while also being much easier to design.

When compared to the return losses of the hand-made power divider in Chapter III, there was a drop in return loss values (max return losses around 25-30 dB instead of 50 dB). However, it should be noted that once 20 dB of return loss is achieved, 99% power is transmitted and any increase in return loss afterwards provides only a minimal improvement (i.e. 99.9% power transmitted vs. 99% power transmitted). More importantly, the improved symmetry of the milled devices eliminated the large frequency shifts between the various return losses seen in the hand-made device and shown in Figure 19. Thus, the port return losses for each milled device achieved desired

performance over a more consistent frequency range than the port return losses for the hand-made device. An interesting characteristic of the port two and port three return losses seen in all four devices is the existence of a second low frequency null. This second null appears at approximately half the center frequency of the port two and port three return losses for each device (approximately 900 MHz for the milled devices and approximately 1200 MHz for the hand-made device). These second null frequency locations indicate a resonance possibly due to phenomena similar to harmonics.

The amplitude balance for each of the power dividers is shown in Figure 30.

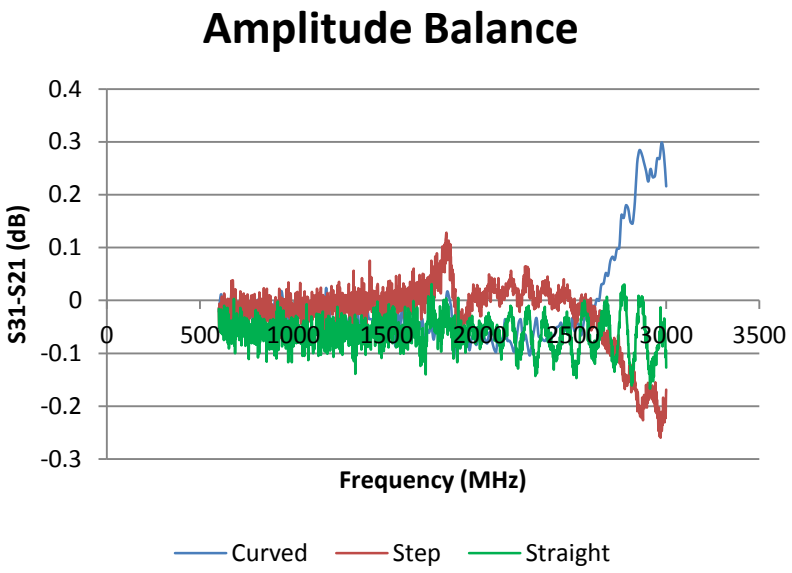

Figure 30: Milled Power Dividers Amplitude Balance

Figure 30 indicates that a nearly identical power split is achieved by each of the power dividers across the entire band (600-3000 MHz). In particular, an amplitude balance between 0.1 and -0.1 is achieved for each device from 600 MHz to approximately 2200 MHz. This further demonstrates the symmetry of each device because S_{21} is essentially equal to S_{31}. Additionally, the amplitude balance values of the milled devices show

significant improvement compared to the hand-made devices (+/- 0.1 dB vs. +/- 0.4 dB). Thus, the symmetry of the milled devices again provides more consistent performance and easily meets typical amplitude balance specifications previously discussed (+/- 0.25 dB)

The values for S_{21} across the band are shown in Figure 31.

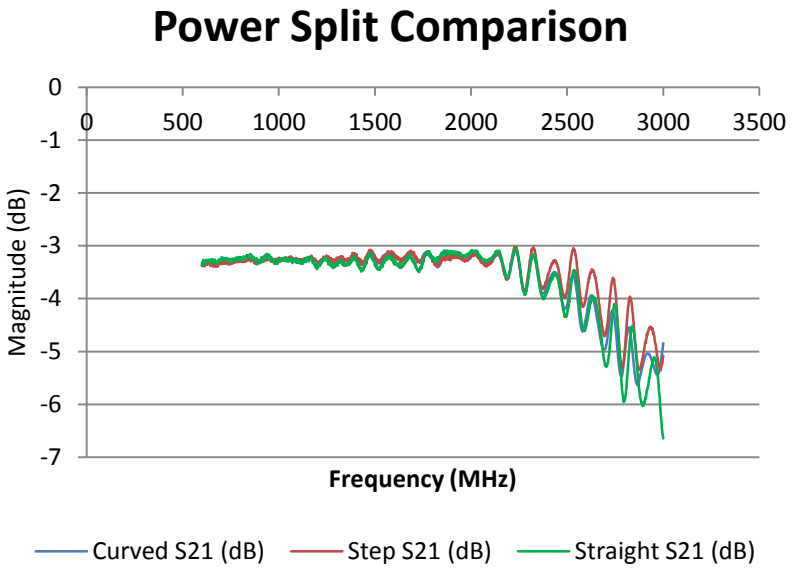

Figure 31: Milled Power Dividers Power Division

Figure 31 indicates that each power divider delivers approximately 47-49% of the input power to the output (3.1-3.3 dB) between 600 and 2200 MHz, or very close to the ideal 50%. The results for S_{31} are essentially the same due to the symmetry of each device as previously explained. These results demonstrate the low loss nature for each of the milled devices, as well as a very similar frequency cutoff for each device (2200 MHz). Each of these devices also shows a much steadier output across the band (3.1-3.3 dB) than the hand-made device (fluctuations between 3.3 and 3.7 dB for port two and 2.8 and 3.4 dB for port three).

The isolation, S_{23}, for each device is shown in Figure 32. Again due to the symmetry of each device, S_{32} is essentially the same as S_{23} and is not displayed in Figure 32.

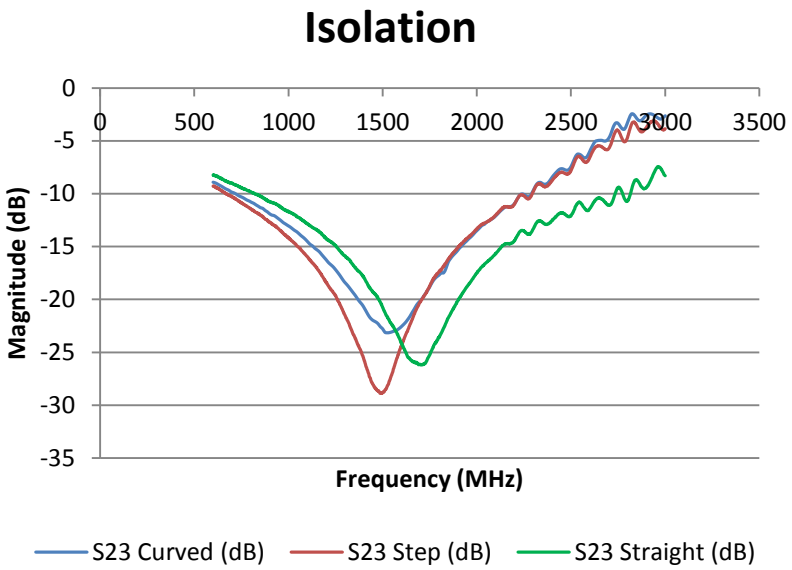

Figure 32: Milled Power Dividers Isolation

The isolation for each of the Wilkinson power dividers is greater than 20 dB with the step divider achieving an isolation close to 30 dB, albeit at a lower frequency (approximately 1500 MHz). Figure 32 also shows that the isolation for the straight power divider is just as good, and in some cases better than the other two curved power dividers, implying that the effects of coupling between the lines in this case is negligible. This is likely due to the 5.28 mm gap between the two quarter-wavelength sections being too wide to introduce a significant amount of coupling between the microstrip lines. These isolation values are comparable to what was seen in the hand-made device, demonstrating that isolation characteristics of various Wilkinson power dividers are minimally affected by device design and construction at this frequency range. Table 11 shows the center

frequency for the isolation of each power divider, the maximum isolation achieved, and the band over which the return loss was greater than 15 dB.

Power Divider	Center Frequency (MHz)	Max Isolation (dB)	Band > 15 dB (MHz)
Curved	1530	23.0	1130-1920
Step	1490	29.0	1050-1905
Straight	1710	26.0	1250-2130

Table 11: Milled Power Dividers Isolation Comparison

As discussed throughout this section, the results of the milled power dividers show a good deal of improvement compared to the initial hand-made power divider, mostly due to the symmetry of each device. The band over which these devices achieved return losses and isolation greater than 15 dB and an amplitude balance within +/- 0.25 dB are shown in Table 12, Table 13, and Table 14.

Parameter	Low Frequency (MHz)	High Frequency (MHz)
S11 Return Loss	1620	2080
S22 Return Loss	600	2230
S33 Return Loss	600	2220
S31/S21 Amplitude Balance	600	2840
S23/S32 Isolation	1130	1920

Table 12: Curved Power Divider Composite Frequency Range

Parameter	Low Frequency (MHz)	High Frequency (MHz)
S11 Return Loss	890	2110
S22 Return Loss	600	2200
S33 Return Loss	600	2200
S31/S21 Amplitude Balance	600	2950
S23/S32 Isolation	1050	1905

Table 13: Step Power Divider Composite Frequency Range

Parameter	Low Frequency (MHz)	High Frequency (MHz)
S11 Return Loss	1690	2160
S22 Return Loss	600	2200
S33 Return Loss	610	2200
S31/S21 Amplitude Balance	600	3000
S23/S32 Isolation	1250	2130

Table 14: Straight Power Divider Composite Frequency Range

These tables indicate that the curved power divider operates ideally between 1620 and 1920 MHz, the step power divider operates ideally between 1050 and 1905 MHz, and the straight power divider operates ideally between 1690 and 2130 MHz. Furthermore, each device meets the necessary performance criteria at 1800 MHz, the intended design frequency. For comparison purposes the scattering matrices at 1800 MHz are shown for each device. It should be noted that these matrices include only the magnitude of the S-parameters.

$$Curved = \frac{1}{\sqrt{2}}\begin{bmatrix} 0.17 & 0.98 & 0.97 \\ 0.97 & 0.10 & 0.18 \\ 0.97 & 0.18 & 0.10 \end{bmatrix} \tag{4.1}$$

$$Step = \frac{1}{\sqrt{2}}\begin{bmatrix} 0.14 & 0.98 & 0.98 \\ 0.97 & 0.09 & 0.19 \\ 0.98 & 0.19 & 0.11 \end{bmatrix} \tag{4.2}$$

$$Straight = \frac{1}{\sqrt{2}}\begin{bmatrix} 0.17 & 0.97 & 0.97 \\ 0.98 & 0.15 & 0.09 \\ 0.97 & 0.10 & 0.13 \end{bmatrix} \tag{4.3}$$

The S-matrices indicate a similar performance between all three devices at 1800 MHz, particularly between the curved and step dividers. One interesting difference however, is that the straight power divider showed lower values for S_{23} and S_{32} than the other two dividers. This indicates a higher isolation value for the straight power divider at 1800 MHz and is easily observed in the isolation plots in Figure 32.

None of the milled devices is significantly better than the others, with each providing a similar performance. However, there are minor differences between the performance of each device that are worth discussing.

It could be argued that the curved power divider shows the weakest performance because it provides the smallest bandwidth, the lowest port one return loss, and lower isolation near 1800 MHz. It was also the most difficult to design with the curves and intricate tapers. The step power divider provided the most bandwidth (900 MHz) due to its port one return loss staying just below 15 dB (approximately 16 or 17 dB) from 890-1500 MHz. The step junction is also easy to incorporate into the design and the rest of its characteristics are comparable to the curved power divider. The straight power divider could actually be considered the best because it operates over a more appropriate band (1690-2130 MHz) for a center frequency near 1800 MHz. It also demonstrated a higher port one return loss than the other devices, a higher isolation value at 1800 MHz, and the straight quarter-wavelength transmission lines were easy to design. In any case, each of these power dividers provides improved performance over the hand-made design, especially considering equal-split power division as the main goal of each device.

Chapter V – Discussion and Conclusions

V.1 Discusssion

Based upon the results in the previous chapters, it is clear that different Wilkinson power divider layouts can achieve very similar results when constructed using microstrip at reasonable frequencies (< 3GHz). This implies that the Wilkinson power divider design features a significant amount of robustness, allowing for a large amount of freedom when determining a microstrip layout. In this thesis it has been shown that a step junction between microstrip sections is just as effective as a taper, resulting in no decrease in return loss. It is also much easier to design and fabricate, better understood in the RF/microwave community, and easily implemented in most simulation software.

Another variation between each design is the thickness of the dielectric for each of the machined devices. Since the depth of the routing machine was set by hand, each device had a slightly different dielectric thickness. However, each device operated similarly, particularly the curved and step power dividers, thus it is likely that the variation in the dielectric thickness had a negligible impact on the overall performance of each device.

Perhaps most intriguing of the previous results was that while circular, curved sections are often implemented in Wilkinson power dividers, the results indicate that parallel microstrip lines can be just as effective and maintain good isolation (>20dB). The following section investigates this phenomenon in more detail to further validate the performance of the straight power divider.

V.2 Coupling and Isolation

Extensive work has been done exploring ways to calculate and model the even and odd mode impedances of coupled microstrip lines. Kirschning and Jansen's equations in particular have been used to solve for these impedances on several occasions and make up the basis for Rogers Corporation's MWI 2010 edge coupled microstrip calculator [21]. The even and odd mode impedances of coupled lines vary as the gap-spacing between them changes. This is due to the capacitance that exists between the lines and ground under each mode of operation. Additionally, as the spacing between the lines decreases, the capacitance, particularly in the odd mode, increases. This results in a lower odd mode impedance. In Pozar's analysis of coupled lines he states that if,

$$Z_0 = \sqrt{Z_{0O} Z_{0E}} \tag{5.1}$$

where Z_0 is the characteristic impedance of each line, and Z_{0O} and Z_{0E} are the odd and even mode impedances respectively, then,

$$C = \frac{Z_{0E} - Z_{0O}}{Z_{0E} + Z_{0O}} \tag{5.2}$$

where C is the coupling coefficient between the lines [1]. Consequently, as the difference between the even and odd mode impedances increases the coupling between the lines increases.

Calculations and simulations were done to further demonstrate this point using Rogers Corporation's MWI 2010 edge coupled microstrip calculator and Sonnet Lite [22]. For both the calculator and the simulation, 4.7 mm wide and 17 μm thick copper conductors were placed over 1.575 mm thick RTDuroid 5870 (essentially, two 50Ω microstrip transmission lines). Due to limitations with Sonnet Lite (port impedances

could not be modified) 50Ω lines were simulated instead of 70.7Ω (the impedance of the quarter-wave sections in the Wilkinson) to ensure a matched system was simulated. Using the Rogers calculator the modal impedances were determined for various gap spaces as shown in Table 15.

Gap Spacing	Z_{0E}	Z_{0O}	Z_{0E} - Z_{0O}
7 mm	50.23	48.11	2.12
5 mm	50.8	47.4	3.4
3 mm	52.13	45.81	6.32
1 mm	55.68	40.81	14.87
0.5 mm	57.32	37.27	20.05
0.1 mm	59.19	30.38	28.81

Table 15: Gap Spacing and Even-Odd Mode Impedances

Table 15 clearly shows that as the gap spacing between the lines decreases, the difference between the impedances increases, thus increasing the coupling. Figure 33 shows the results for the coupling between the transmission lines simulated in Sonnet Lite (the layout of these simulated transmission lines is shown in Figure 36) and further validates the trends indicated by the Rogers calculator.

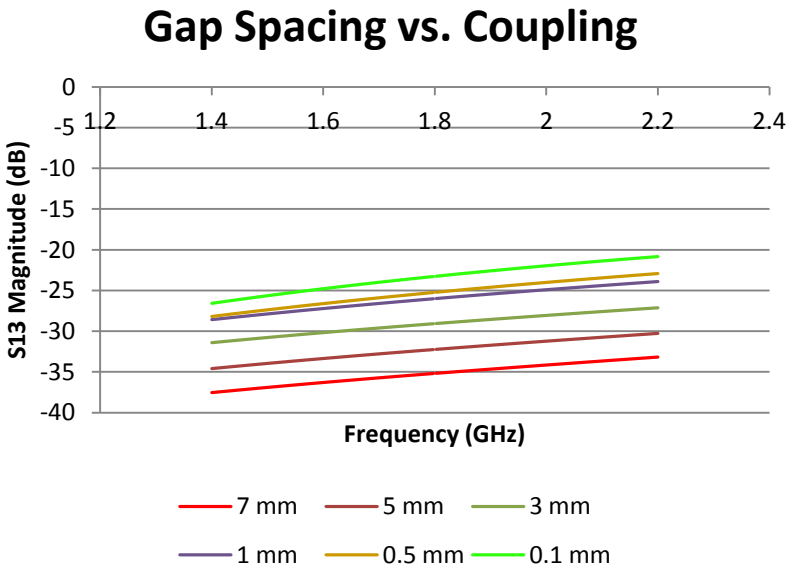

Figure 33: Gap Spacing vs. Coupling: Sonnet Simulation

As previously discussed, the isolation of a power divider is an important aspect of its operation. Figure 34 indicates how the isolation between two coupled lines decreases as the gap spacing increases.

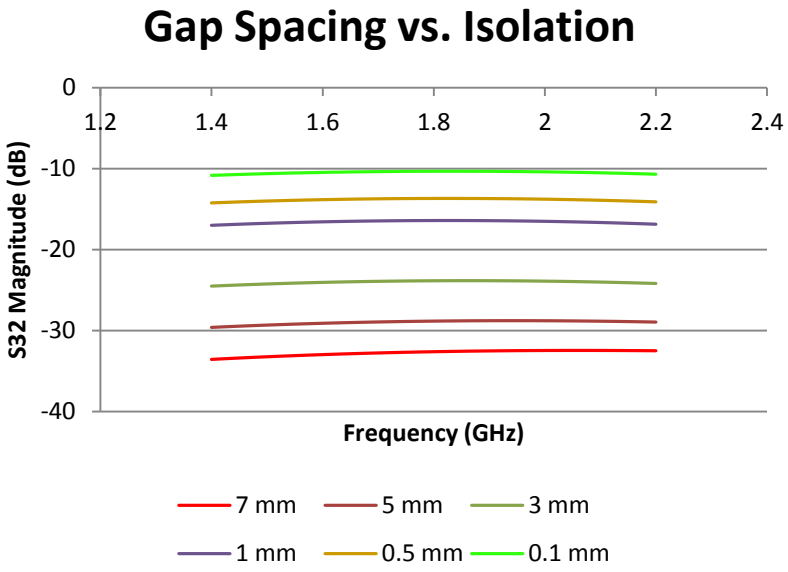

Figure 34: Gap Spacing vs. Isolation: Sonnet Simulation

As shown in Figure 34, the two 50Ω transmission lines simulated in Sonnet achieved an isolation around 28-30 dB for a 5 mm gap spacing over the simulated frequency range. Although these are stand-alone transmission lines at a different impedance than the quarter-wave sections in each of the constructed Wilkinson power dividers, the results are still comparable to those measured from the straight power divider (the straight power divider achieved a maximum isolation of 29 dB within this frequency range). These simulation results also indicate that a gap spacing of 1 mm or less would likely have to be used to bring the isolation of the Wilkinson below 15 dB for a majority of the measured frequency range. Figure 35, Figure 36, Figure 37, and Figure 38 show how the current

density on each transmission line changes as the gap space decreases from 5 mm to 0.1 mm.

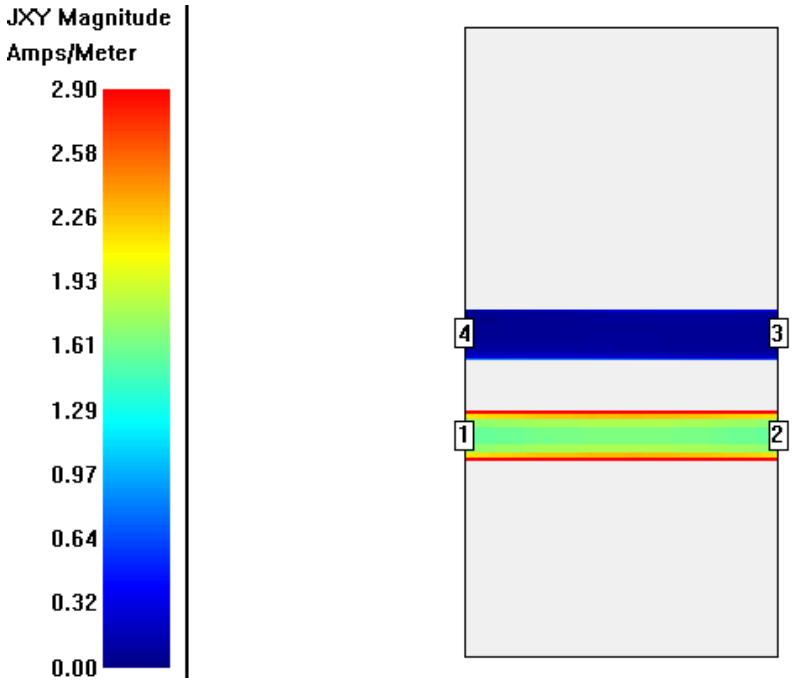

Figure 35: 5 mm Gap – Current Density Sonnet Simulation

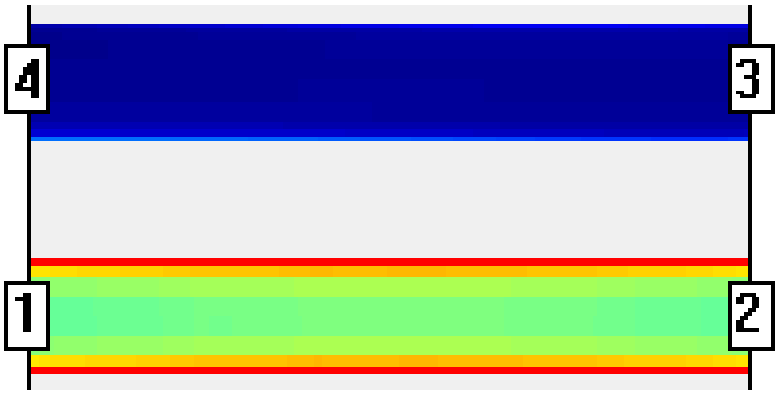

Figure 36: 5 mm Gap – Current Density Zoomed In

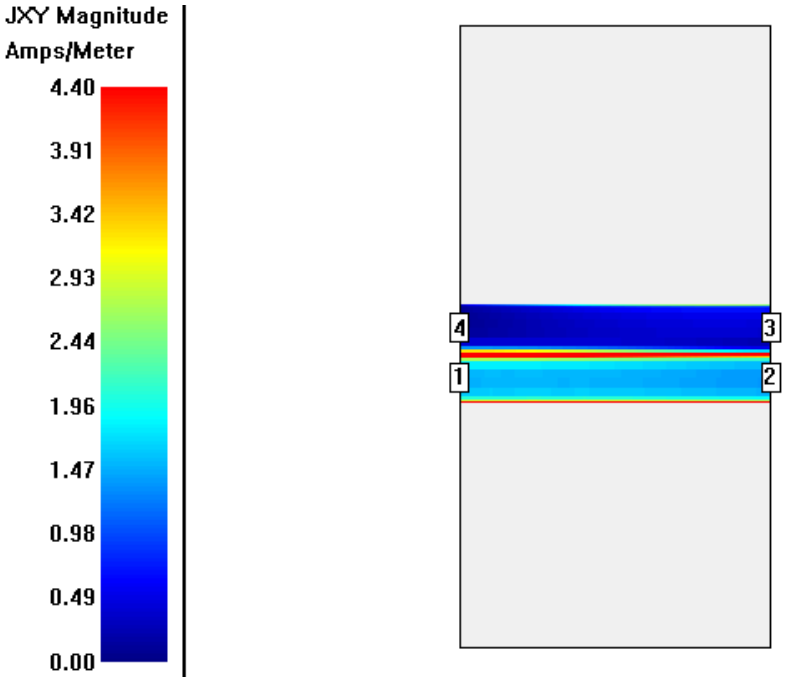

Figure 37: 0.1 mm Gap – Current Density Sonnet Simulation

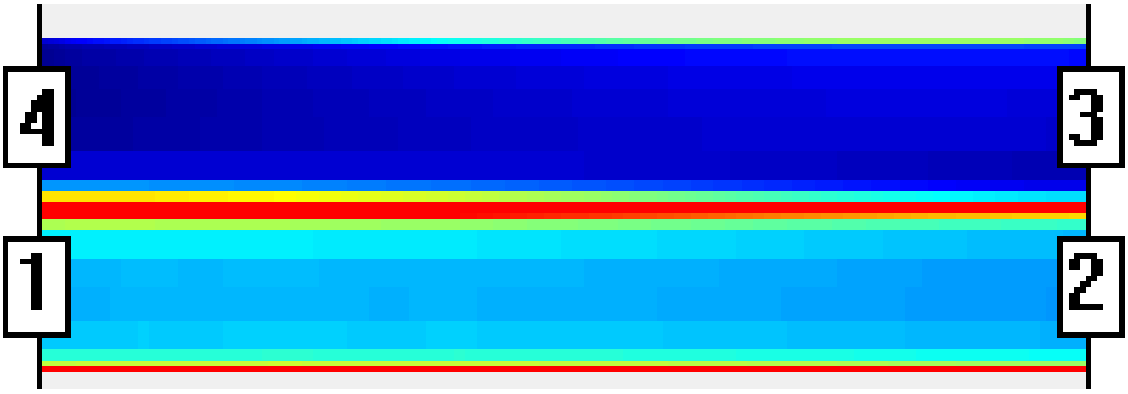

Figure 38: 0.1 mm Gap – Current Density Zoomed In

These figures show how essentially no current is coupled to the second transmission line when the gap between the lines is 5 mm. It is also interesting to see that even with a gap spacing of 0.1 mm, there is only a small amount of coupling and isolation values of 10 dB can still be achieved.

It should be noted that the effects of coupling between transmission lines for the equal-split Wilkinson power divider come into play when the reflections from the output

ports are large or when the device is being used as some type of combiner. Equal-split power division implies the transmission lines are under the even mode of operation and the signals traveling along each transmission line have near equal amplitude and phase regardless of gap spacing. Figure 39 shows that when a source is applied at both ports 1 and 4 (even mode operation) the currents along each transmission line are essentially identical even with a gap spacing of 0.1 mm.

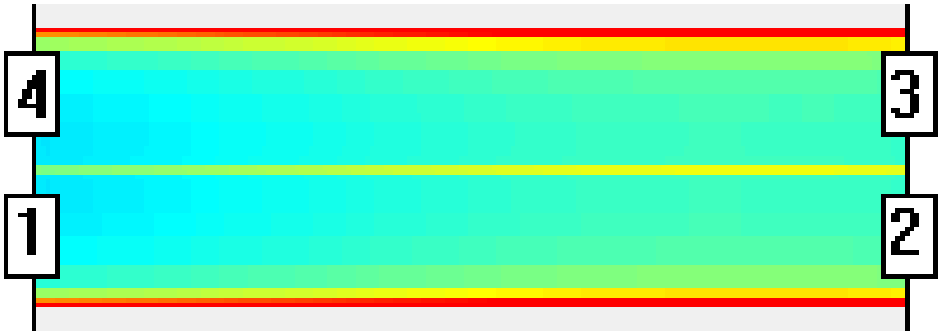

Figure 39: 0.1 mm Gap – Even Mode Operation

V.3 Conclusions and Future Work

The work presented in this thesis indicates that Wilkinson power dividers are very robust devices, and different designs can achieve similar performance, particularly when constructed using simple microstrip fabrication techniques and operating at reasonable frequencies. Although the Wilkinson is a narrowband device, bandwidths up to 900 MHz were achieved using relatively simple designs, while also meeting typical manufacturing performance criteria (15 dB return losses, 15 dB isolation, and 0.25 dB amplitude balance).

It has also been shown that although the curved quarter-wave sections are often implemented in Wilkinson power dividers, straight quarter-wave sections can be just as effective and minimize the width of the power divider. This is of particular importance

because a Wilkinson power divider with a much simpler microstrip layout can be designed and constructed without fear of performance degradation. Furthermore, the negative effects of coupling between the quarter-wavelength sections were shown through simulation to have a significant impact on power divider isolation at gap widths less than 1 mm. Consequently, by keeping the gap width between quarter-wave sections greater than 1 mm for Wilkinson power dividers operating below 3 GHz, typical isolation values (>15 dB) can still be achieved.

Another conclusion drawn from this thesis is that the step junction is just as effective as a taper. The step junction is a well understood microstrip discontinuity and is easily implemented in microstrip simulation programs. The results from the previous chapter indicate that step junctions provide similar performance (no degradation in return losses) to tapers at frequencies below 3 GHz. These results are consistent with claims from the RF/microwave community [12].

Hand-made devices, although feasible, require careful cutting techniques to maximize the symmetry of the Wilkinson. The symmetry of the device appears to be the most critical aspect of the design and construction, particularly for an equal-split power divider. As the results from the hand-made divider indicate, a slight lack of symmetry can result in various return loss frequency shifts and larger than desired amplitude balance values.

The actual power handling capabilities of each of the constructed power dividers is limited by the one watt resistor. Consequently, each of these devices is only suitable for low power applications, and a topic for future exploration includes the power handling limitations of microstrip Wilkinson power dividers. Although each constructed

Wilkinson power divider takes up a footprint no bigger than 2” x 3”, much smaller power dividers operating at similar frequencies are still an area of active research [23]. Furthermore, the effects of coupling between transmission lines and how these effects can be used to further decrease power divider footprint is a topic that could also be more thoroughly investigated [9]. The Wilkinson power divider is, in its most basic form, a relatively simple yet incredibly effective RF device. As discussed in this thesis, there are a seemingly infinite number of ways to tweak this simple design, and different designs can achieve the same goals. Research on the Wilkinson power divider and its various forms should continue for years to come and the results will be warmly received.

BIBLIOGRAPHY

[1] D. Pozar, *Microwave Engineering*, 3rd ed. Hoboken, New Jersey: John Wiley & Sons Inc. pp. 308-361, 2005.

[2] A. Grebennikov, *RF and Microwave Transmitter Design*, Hoboken, New Jersey: John Wiley & Sons Inc. 2011.

[3] K. Chang, *Encyclopedia of RF and Microwave Engineering*, Hoboken, New Jersey: John Wiley & Sons Inc. 2005.

[4] E. J. Wilkinson, "An N-Way Hybrid Power Divider," *IRE Transactions on Microwave Theory and Techniques*, Vol. 8 Issue 1, pp. 116-118, 1960.

[5] Y. Konishi, *Microwave Electronic Circuit Technology*, New York, New York: Marcel Dekker Inc. pp. 273-292, 1998.

[6] J. Li, "Novel Design of Wilkinson Power Dividers With Arbitrary Power Division Ratios," *IEEE Transactions on Industrial Electronics*, Vol. 58 Issue 6, pp. 2541-2546, 2011.

[7] L. Wu, Z. Sun, H. Yilmaz, and M. Berroth, "A Dual-Frequency Wilkinson Power Divider," *IEEE Transactions on Microwave Theory and Techniques*, Vol. 54 Issue 1, pp. 278-284, 2006.

[8] A. Wentzel, V. Subramanian, A. Sayed, and G. Boeck, "Novel Broadband Wilkinson Power Combiner," *Proceedings of the 36th European Microwave Conference*, pp. 212-215, 2006.

[9] X. Tang and K. Mouthaan, "Analysis and Design of Compact Two-way Wilkinson Power Dividers Using Coupled Lines," *APMC, Singapore* pp. 1319-1322, 2009.

[10] J. Stiles, "The Wilkinson Power Divider," University of Kansas, Dept. of EECS, 2009, http://www.ittc.ku.edu/~jstiles/622/handouts/The%20Wilkinson%20Power%20Divider.pdf, accessed 2012.

[11] D. Cheng, *Field and Wave Electromagnetics*, 2nd ed. Reading, Massachusetts: Addison-Wesley Publishing Company pp. 388-400, 1983.

[12] T. C. Edwards, *Foundations of Interconnect and Microstrip Design*, 3rd ed. West Sussex, England: John Wiley & Sons Ltd. pp. 83-112, 2000.

[13] E. O. Hammerstad, "Equations for Microstrip Circuit Design," *Proceedings of the 5th European Microwave Conference*, pp. 268-272, 1975.

[14] E. O. Hammerstad and O. Jensen, "Accurate Models for Microstrip Computer-Aided Design," *IEEE MTT-S International Symposium Digest*, pp. 407-409, 1980.

[15] Roger Corporation MWI-2010, http://www.rogerscorp.com/acm/technology/index .aspx, accessed 2012.

[16] T.G. Bryant and J.A.Weiss, "Parameters of Microstrip Transmission Lines and Coupled Pairs of Microstrip Lines," *IEEE Transactions on Microwave Theory and Techniques*, Vol. 16 Issue 12, pp. 1021-1027, 1988.

[17] H.A. Wheeler, "Transmission Line Properties of Parallel Strips Separated by a Dielectric Sheet," *IEEE Transactions on Microwave Theory and Techniques*, Vol. 13 Issue 2, pp. 172-185, 1965.

[18] M.V. Schneider, "Microstrip Lines for Microwave Integrated Circuits," *The Bell System Technical Journal*, pp. 1421-1444, 1969.

[19] Microwave Power Divider and Couplers Tutorial, Marki Microwave, Inc. Morgan Hill, CA. http://www.markimicrowave.com/menus/appnotes/microwave_power_dividers _and_couplers_primer.pdf, accessed 2012.

[20] PD1020 – Power Divider/Combiner, InStock Wireless Components, http://www.instockwireless.com/power_divider_pdf/power_divider_pd1020_7.pdf, accessed 2012

[21] M. Kirschning and R. H. Jansen, "Accurate Wide-Range Design Equations for the Frequency-Dependent Characteristic of Parallel Coupled Microstrip Lines," *IEEE Transactions on Microwave Theory and Techniques*, Vol. 32 Issue 1, pp. 83-90, 1984.

[22] *Sonnet Users Manuals*, Sonnet Software Inc., Syracuse, NY, 2011, release 13.55.

[23] M. Alkanhal, "Reduced-Size Dual Band Wilkinson Power Dividers," *Proceedings of the International Conference on Computer and Communication Engineering*, pp. 1294-1298, 2008.